

Physics of multicellular systems

From cell to tissue mechanics

Hervé Turlier

July 27, 2023

Contents

1 From cell to tissue tension	2
1.1 Preliminaries [1]	2
1.1.1 Origin of liquid surface tension	2
1.1.2 Force balance: Laplace and Young-Dupré laws	3
1.2 Surface tension of a tissue	4
1.2.1 Steinberg's differential adhesion hypothesis	4
1.2.2 Tension measurement	6
1.3 Origin of tissue tension	9
1.3.1 Differential Adhesion vs Tension Hypothesis	9
1.3.2 Cortical tension and adhesion coupling	11
1.3.3 L. Manning's model of tissue tension	11
2 Vertex models of tissues	18
2.1 2D vertex models of epithelial tissues	18
2.1.1 Topology	19
2.1.2 2D vertex model	20
2.2 3D vertex models	23
2.2.1 Epithelial 3D vertex model	23
2.2.2 Non-epithelial 3D vertex models	24
3 Continuous models of tissues - dissipation and nematic order	39
3.1 Preliminary: continuum mechanics, a minimal introduction	39
3.2 Tissues as active fluids	41
3.2.1 Active gel theory	41
3.2.2 Application: spontaneous flow in a confined epithelium	47
3.2.3 Topological defects	50
4 Continuous models of tissues - tissue growth	57
4.1 Unconstrained growth of a spheroid	57
4.1.1 Population dynamics	57
4.1.2 Application: growth of an incompressible spheroid	58
4.2 Coupling between stress and proliferation	59
4.2.1 Homeostatic pressure	59
4.2.2 Application: expansion of a proliferating confined tissue	60

Chapter 1

From cell to tissue tension

Multicellular aggregates generally adopt a spherical shape, which resembles the one of a liquid droplet. This suggests that tissues may have a surface tension. This idea was further developed by M. Steinberg in the 1960's [2].

1.1 Preliminaries [1]

1.1.1 Origin of liquid surface tension

Surface tension is, by definition, an energy per unit surface. Its unit is therefore $\text{J.m}^{-2} = \text{N.m}^{-1}$. In physics, it is commonly denoted by the symbol γ .

Surface tension is generally associated to liquid surfaces, and quantifies by essence, the fact that an interface between two immiscible phases costs an energy that is proportional to the interface area:

$$\delta\mathcal{E} = \gamma\delta A \quad (1.1)$$

At a given volume, the minimal surface of an isolated material is the sphere, which explains the spherical shape of droplets, bubbles etc...

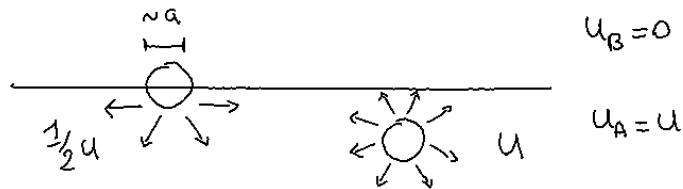


Figure 1.1: Origin of surface tension between a liquid and air.

Between two liquids A and B (or between a liquid A and a gaz B), a surface tension emerges from the different cohesion energies. In the limit of a gaseous phase B, we assume the cohesion energy U_B of molecules B to be zero., while the cohesion energy of molecules A is $U_A = U > 0$. The following sketch shows graphically that surface tension is due to the loss of one half of the cohesion between A molecules at the interface between phases A and B.

If the size of the molecule A is a , the surface tension may be simply deduced as half of cohesion energy

divided by the typical surface a^2 of a molecule:

$$\gamma \sim \frac{1}{2} \frac{U}{a^2} \quad (1.2)$$

Examples of typical values of surface tension in the nature

- $\gamma_{\text{water}} \sim 72 \text{ mN.m}^{-1}$ for water/air interface at 25°C
- $\gamma_{\text{mercury}} \sim 486 \text{ mN.m}^{-1}$ for mercury/air interface at 25°C

1.1.2 Force balance: Laplace and Young-Dupré laws

Laplace's law

For an isolated droplet, there is only one relevant force balance equation, which is projected along the normal to the surface, and is named after Laplace. Laplace's law relates the difference of pressure between the inside and outside compartments P_{int} and P_{ext} , the surface tension γ and the curvature radius R by

$$\Delta P = P_{\text{int}} - P_{\text{ext}} = \frac{2\gamma}{R} \quad (1.3)$$

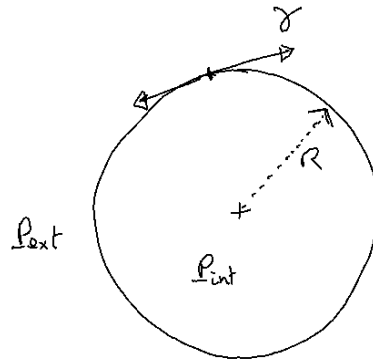


Figure 1.2: Laplace's law

The factor 2 stems from the fact that there are two principal curvature radii $R_1 = R_2 = R$, which are equivalent in a sphere. A generalized Laplace's formula for more complicated shapes and possibly for different tensions along the two principal curvature radii would read

$$P_{\text{int}} - P_{\text{ext}} = \frac{\gamma_1}{R_1} + \frac{\gamma_2}{R_2} \quad (1.4)$$

Wetting parameter and Young-Dupré's law

When a droplet enters in contact with a surface, it may adhere (generally partially) to it. One can define generically three surface tensions between the three phases (air, water, solid):

- $\gamma_{aw} = \gamma$ for the surface tension between air and water
- γ_{as} for the tension between air and solid
- γ_{sw} for the tension between the solid and water

The relevant parameter to measure the degree of droplet adhesion onto the surface (or spreading/weeting) is called a wetting (or spreading) parameter, defined as

$$S = \gamma_{as} - (\gamma_{sw} + \gamma) \quad (1.5)$$

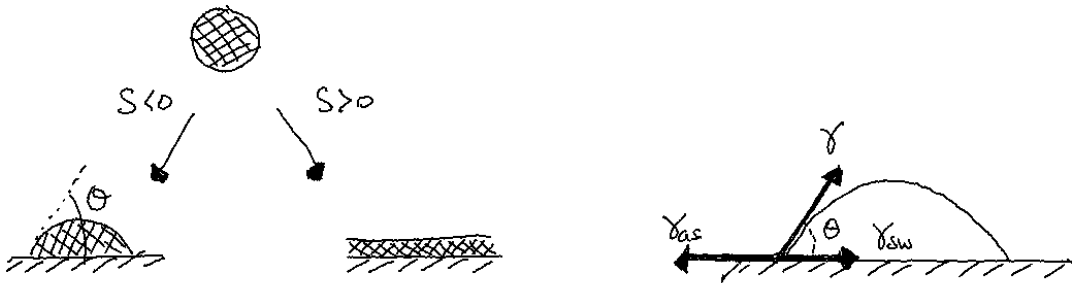


Figure 1.3: Total and partial wetting (left) and Young Dupré law (right)

- If $S > 0$ wetting is said to be total: the contact angle is zero and the droplet spreads onto the solid surface until forming a nanoscopic layer of fluid called precursor layer.
- If $S \leq 0$ wetting is partial, and the droplet contacts the solid substrate with an angle θ .

For partial wetting, the contact line follows Young-Dupré's tension balance, which may be expressed in a vectorial form:

$$\vec{\gamma} + \vec{\gamma}_{sw} + \vec{\gamma}_{as} = \vec{0} \quad (1.6)$$

or projecting onto the flat substrate, may also be expressed as function of the contact angle θ

$$\gamma \cos \theta = \gamma_{as} - \gamma_{sw} \quad (1.7)$$

1.2 Surface tension of a tissue

1.2.1 Steinberg's differential adhesion hypothesis

The differential adhesion hypothesis of Steinberg states that tissues have a tension (because they adopt spherical shapes in isolation) and that this tension is controlled by the cohesion (or adhesion) energy of cells within the tissue, in direct analogy with the physics of liquids.

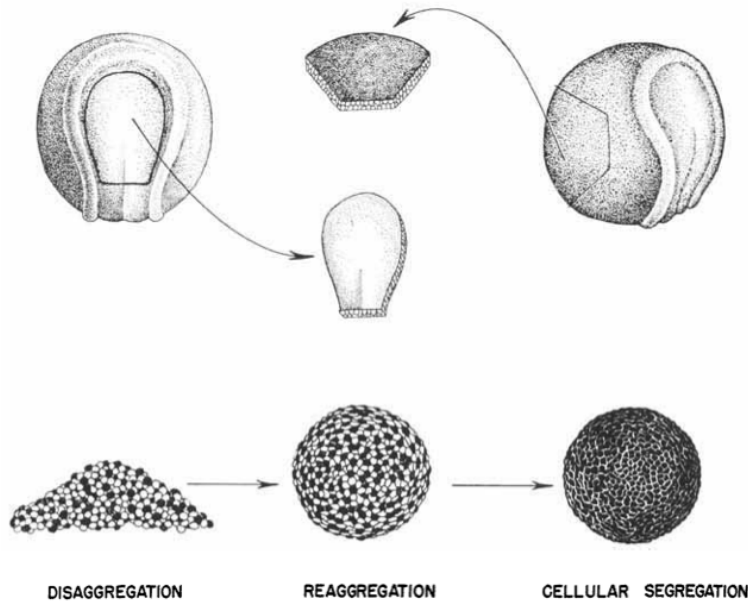


Figure 1.4: Sketch of the early experiments by Holtfreter [3]

This hypothesis was directly inspired by early experiments made by Holtfreter with fragments of amphibian embryos [3], where cells from endoderm and ectoderm precursor tissues were disaggregated and reaggregated. Forming a mixture, the resulting aggregate not only rounds up but the cells of different types also spontaneously sort out, with ectoderm cells at the exterior and endoderm cells in the interior, as naturally observed in the embryo (see Fig. 1.4). Later on, Steinberg performed a series of related experiments [2, 4] with various tissues to confirm that this behavior is generic and is directly correlated with a measurable tension of the tissue, and that such tissue tension is directly proportional to the amount of adhesion molecules between cells [5].

To quantitatively verify the differential adhesion hypothesis, Steinberg compares experiments with predicted configurations of minimal surface energy for a binary mixture of two liquids A and B, characterized by homophilic cohesion energy densities w_A and w_B (between phases of same nature) and an heterophilic adhesion energy density w_{AB} (between phases of different nature) [2].

In general, one expects the free energy of the system to read

$$\mathcal{F} = - \int_{S_{AB}} w_{AB} dS - \int_{S_A} w_A dS - \int_{S_B} w_B dS \quad (1.8)$$

where S_{AB} is the area of heterophilic contacts between cells of types A and B, and S_A and S_B the area of contact between cells of same type, either A or B.

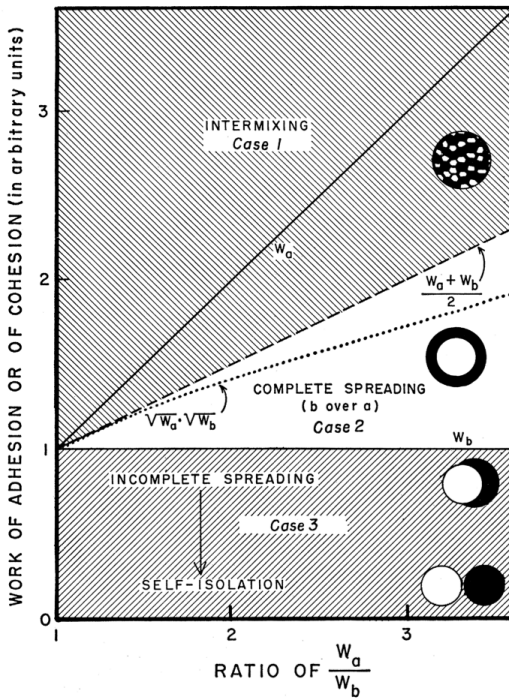


Figure 1.5: Phase diagram of the minimum energy configuration of binary mixture of cells of type A and B [2]

One may distinguish two main cases:

- If $w_{AB} \geq \frac{w_A + w_B}{2}$, one expects the energy to be minimum when the tissue forms a perfectly alternating mixture of cells A and B, which corresponds to the Case 1 in Fig. 1.5.
- If $w_{AB} < \frac{w_A + w_B}{2}$, one may expect, on the contrary, cells of type A and B to segregate in separated compartments. Several scenario are however possible in this case:
 1. If one supposes furthermore that the adhesion strength between A and B cells is higher than between cells of type B themselves $w_{AB} \geq w_B$. This implies $\frac{w_A + w_B}{2} > w_{AB} \geq w_B$, which is possible only when $w_A > w_{AB} \geq w_B$. In such situation, where the cohesion strength of B is of

lesser extent, will tend to have it at the exterior, while A will tend to be inside the spherical aggregate, which corresponds to the complete spreading (Case 2 of Fig. 1.5).

2. If, on the contrary, one supposes $w_A \geq w_B > w_{AB}$, spreading is expected to be incomplete, corresponding to Case 3 on Fig. 1.5. In the limit of vanishing adhesion between A and B, one expects two separated isolated spherical aggregates.

1.2.2 Tension measurement

Parallel plates tensiometer

To quantitatively assess the predictions above, Steinberg and his collaborators have developed a tissue tensiometer based on the compression between two parallel plates [4, 6].

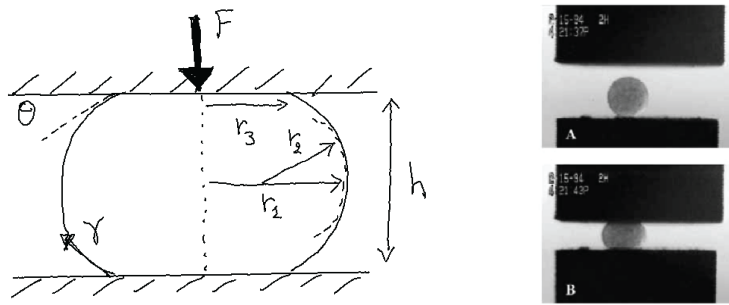


Figure 1.6: Parallel plate tensiometer

A compressive force F is applied by the upper plate on the tissue, that deforms and increases its pressure to resist the deformation and conserve its volume. The geometrical parameters describing the deformed tissue from a sphere are depicted on the Fig. 1.6.

Normal force balance on the contact surface between the cell aggregate and one plate reads

$$F + \gamma 2\pi r_3 \sin \theta = \Delta P \pi r_3^2 \quad (1.9)$$

In the midplane of the aggregate, where principal curvature radii are r_1 and r_2 , Laplace's law reads furthermore $\Delta P = \gamma \left(\frac{1}{r_1} + \frac{1}{r_2} \right)$, leading to the following formula for the tissue tension

$$\gamma = \frac{F}{\pi r_3^2} \left(\frac{1}{r_1} + \frac{1}{r_2} \right)^{-1} \quad (1.10)$$

In [5, 6], geometric approximations are made, which consists in assuming circular arc shapes for the lateral tissue profile. If there is no adhesion between the tissue and the plate ($\theta = 0$), then $r_2 \sim \frac{h}{2}$ and $r_3 = r_1 - r_2$. If the tissue and the plate have a non-zero (partial) adhesion ($\frac{\pi}{2} > \theta > 0$), one may calculate r_3 from Pythagore theorem, yielding $r_3 = (r_1 - r_2) + \sqrt{r_2^2 - (\frac{h}{2})^2}$. The optical determination of the contact angle θ is however generally tedious and imprecise.

In fact, the shape of lateral tissue profile shall not be circular, as the surface shall be of constant mean curvature following Laplace's law. The true profile is called an onduloid (or hyperbolic roulette), and the correct formula for the tension based on the exact solution of Laplace's equation was derived in [7].

Micropipette aspiration

An alternative technique to measure the surface tension of a liquid-like cell aggregate is the aspiration in a micropipette. The technique was developed by Mitchison and Swann in the 1950's to measure the surface tension of individual cells, and they called it *cell elastimeter* [8]. It consists in aspirating a portion of a

cell into a micropipette by applying a drop of pressure inside the pipette and to measure the length of the aspirated cap.

Following the original manuscript's notation (see Fig. 1.7, we define R the radius of the cell, d the diameter of the pipette, x the length of the aspirated length and r the curvature radius of the aspirated spherical cap.

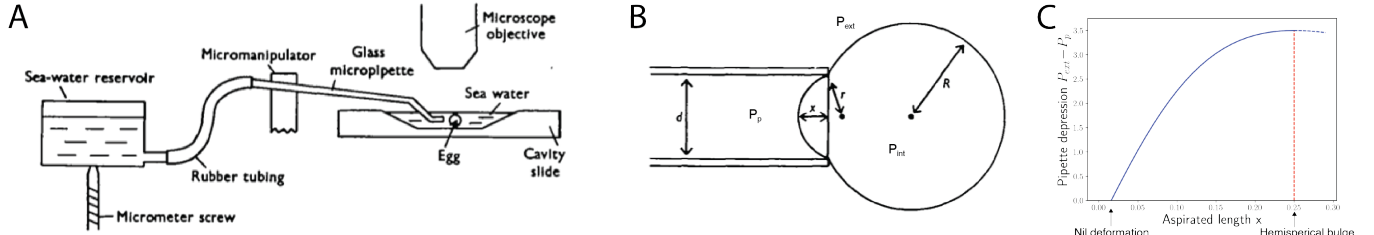


Figure 1.7: Micropipette aspiration: (A) General arrangement of the cell elastimeter. (B) Geometric parametrization of the problem. (C) Plot of the depression in the pipette as function of the aspirated cell cap length x [8].

Denoting γ the surface tension of the cell, P_{int} the pressure inside the cell, P_{ext} the pressure of the external medium, and P_p the pressure inside the pipette, we may write Laplace's law at the interface between the cell and the external medium $P_{int} - P_{ext} = 2\gamma/R$ and between the cell and the pipette $P_{int} - P_p = 2\gamma/r$. Combining the two equations we obtain the pressure drop in the pipette as function of the cell geometry $P_{ext} - P_p = 2\gamma \left(\frac{1}{r} - \frac{1}{R} \right)$.

Using Pythagore theorem, we furthermore have $r^2 = (d/2)^2 + (r - x)^2$, such that

$$P_{ext} - P_p = 2\gamma \left(\frac{2x}{x^2 + d^2/4} - \frac{1}{R} \right) \quad (1.11)$$

The pressure drop in the pipette may be plotted as function of x as shown on Fig. 1.7C, assuming that R remains approximately constant (small pipette). The tension may be deduced by fitting the linear part of this curve

In the limit case, where $x \sim r \sim d/2$ (which is often used experimentally, although the cell configuration becomes metastable), one gets simply $P_{ext} - P_p \sim 2\gamma \left(\frac{2}{d} - \frac{1}{R} \right) \equiv \Delta P_c$, where ΔP_c is often called "critical" pressure. Above the critical pressure, the cell will as the pressure difference in the pipette decreases with the length of the aspirated cell portion.

This technique was recently applied to spherical cell aggregates by Guevorkian et al. [9]. The tension value they measured is $\gamma \approx 6 \text{ mN.m}^{-1}$ for murin sarcoma cells (S180). In this study, they did not only measure the tension of the tissue but by measuring the speed of the entry of the cell tongue inside the micropipette, they could also extract viscoelastic parameters characterizing the aggregate.

Magnetic tensiometer

Recently, an original method [10] was developed to measure the tension of a tissue by a method mimicking the so-called sessile drop tension measurement (see Fig. 1.8). A sessile drop is of radius larger than the capillary size¹ $\kappa^{-1} \sim \sqrt{\frac{\gamma}{\rho g}}$, and will be flattened by gravity. The profile of the drop results from the competition between gravity and surface tension forces, and its fitting may allow to come back to a numerical evaluation of the fluid surface tension. However, for tissues, this capillary size is of the order of $\sim \sqrt{\frac{10^{-2}}{10^3 \times 10}} = 1 \text{ mm}$, while typical cell aggregates generated *in silico* are generally also of maximum size $100 \mu\text{m} - 1 \text{ mm}$ which does not lead to large deformations allowing for direct application of the sessile drop method. Therefore, the

¹The capillary size compares the Laplace's pressure created by the surface tension $\sim \gamma/\kappa^{-1}$ and the hydrostatic pressure created by gravity $\sim \rho g \kappa^{-1}$ (with ρ the fluid density and g the gravitational field strength on Earth).

authors have got the idea to incorporate ferromagnetic nanoparticles into cells, and to generate a magnetic field gradient to create a bulk magnetic force in cells along the vertical direction of magnitudes up to ~ 150 g. The typical magnetic force per unit volume they generate is $\vec{f}_v = \nabla(\vec{M}_v \cdot \vec{B}) \sim 10^5 \text{ N.m}^{-3}$, and they measure typical tissue surface tensions $\gamma \sim 10 \text{ mN.m}^{-1}$ [10, 11].

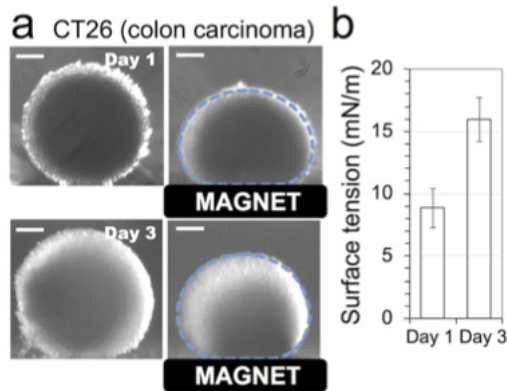


Figure 1.8: Magnetic tensionmeter: (a) Profiles of cell aggregates before and after application of the magnetic field gradient. (b) Typical values of tensions measured after 1 and 3 days [11].

1.3 Origin of tissue tension

1.3.1 Differential Adhesion vs Tension Hypothesis

After the initial differential adhesion hypothesis (DAH) of Steinberg [2], a long physical debate has animated the community about the true physical origin of the surface tension in a tissue. One of the first author to openly criticize Steinberg's hypothesis is Albert K. Harris in a long discussion [12], where alternative explanations for the emergence of a tissue tension are proposed. In contrast to the assumption that cells would behave exactly like molecules in a fluid, Harris promotes the notion of differential contraction (or differential contractility hypothesis DCH) as the most likely explanation of tissue sorting phenomena. His idea is based on the fact that cells are known to have a contractile surface that generates also a surface tension at the cell level, that may be controlled by several cellular processes,. In particular, contractility may be reduced at cell-cell interfaces but may also depend on the cell type. In this scenario, the rounding up of aggregates may be explained by the formation of a (more) contractile layer composed of the exposed portions of cells located at the aggregate surface. The contraction of this surface layer would minimize the exposed surface area and round up the aggregate. Similarly, the engulfment of one aggregate into another may be explained by a differential of contractility between them, where the more contractile aggregate will gradually pull the other aggregate around it. One difficulty that Harris raises is the difficulty to differentiate the DAH from the DCH, although he predicts that inhibiting contractility by drugs depolymerizing the cortical layer could lead to large decrease in tissue tension, that could not be explained by the DAH.

First numerical simulations of cell sorting used were realized by Graner and Glazier using Potts models [13] (Monte Carlo simulations on a fixed grid) and could realistically simulate the process of sorting starting from an initial configuration with randomly assigned cell types (see Fig. 1.9A).

More recently, G. Wayne Brodland proposed to replace the concept of DAH or DCH by the concept of differential interfacial tension hypothesis (DITH), which may encompass both effects of adhesion energy and contractile tension by defining cells configuration through the balance of interfacial tensions [14]. Performing 2D simulations using finite elements, Brodland could reproduce and characterize many of the observations of partial and total engulfment observed in 3D tissues (see Fig. 1.9B).

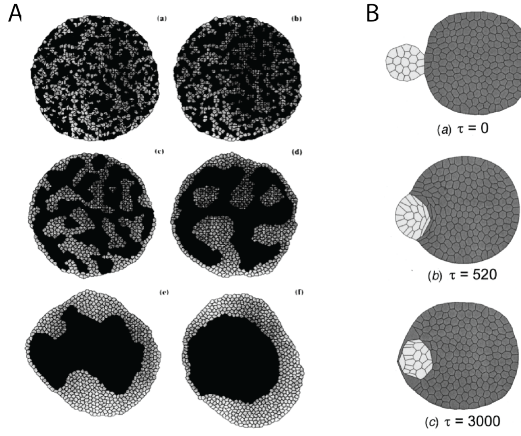


Figure 1.9: Simulations of sorting: (A) Potts simulations of cell sorting [13]. (B) Finite-element simulations of tissue engulfment [14].

1.3.2 Cortical tension and adhesion coupling

The fact that cells in suspension are round is a strong sign of a surface tension. But where is this tension coming from? The surface of cells is composed of plasma membrane (lipid bilayer), which separates topologically the cell interior and exterior, to which is attached a cortical layer made of a thin network of semi-flexible polymer filaments (a few 100nm thick). These filaments called actin are under fast renewal (about 30s to 1min turnover time), are crosslinked by various proteins (α -actinin, plastin, fascin, filamin, Arp2/3...) and put under tension by minifilaments of molecular motors called myosins (see Fig. 1.10A). The activity of molecular motors creates a contractile stress in this gel, that results into an effective surface tension called cortical tension. The tension γ_{cell} at the surface of a cell is therefore generically the result of two contributions a cortical tension $\gamma_{\text{cortex}} \sim 100\text{pN}/\mu\text{m}$ and a membrane tension $\gamma_{\text{membrane}} \sim 10\text{pN}/\mu\text{m}$. The latter is generally an order of magnitude lower than the cortical tension, such that most of the tension at the cell surface may be attributed to the cortical contractility.

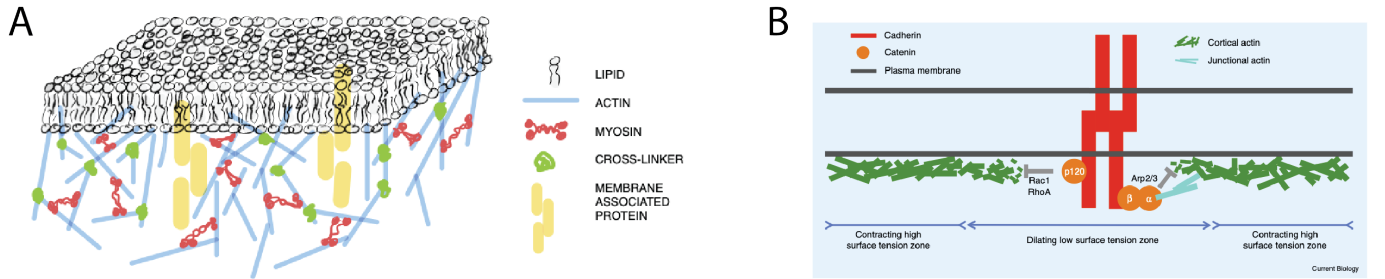


Figure 1.10: (A) Sketch of the cell surface with the lipid bilayer and cortical components [15]. (B) Sketch of the negative feedback mechanism of cell adhesion through cadherins onto the cell cortex [16].

The recent experiments in the field confirm Harris's hypothesis that contractility is the main origin of tissue tension and that sorting phenomena relies on differential interfacial tension [17]. The main idea is that adhesion couples mechanically cell surfaces and decreases contractility at interfaces through negative signaling feedback from bound cadherin adhesion molecules to the cortex (see Fig. 1.10B).

Yet there is still no complete generic consensus on the absolute contribution of the adhesion energy [16]. Generically, defining the tension γ_{cm} at a free interface in contact with the cell medium, one may define the tension at a cell-cell contact $\gamma_{\text{cc}} \sim 2\beta\gamma_{\text{cm}} - W$, where W is the direct negative energetic contribution arising by the binding of adhesion molecules and β measures the degree of cortical depletion at cell-cell interfaces.

From the knowledge of the tensions γ_{cm} and γ_{cc} , one can generically predict the configuration of a cell doublet.

1.3.3 L. Manning's model of tissue tension

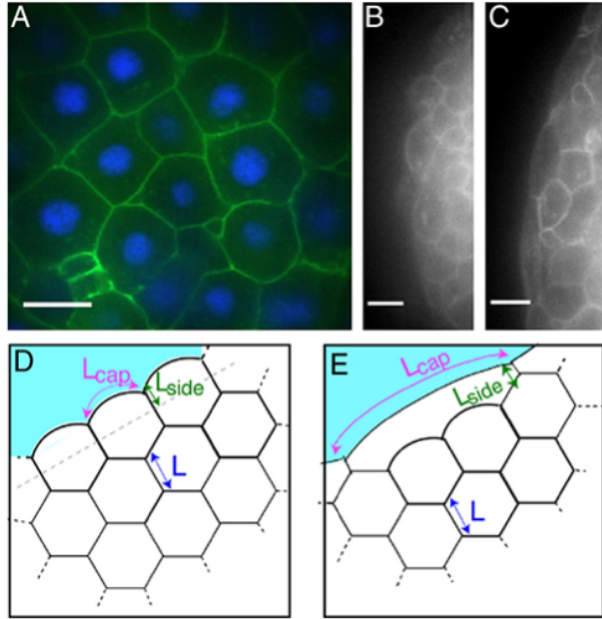


Figure 1.11: (A) Confocal section of a zebrafish aggregate. (B) Surface cells where E-cadherin is down-regulated. (C) Surface cells of an ectoderm aggregate. (D) and (E) Corresponding schematics of cell arrangement and shape.: cells at the surface maintain a compact shape (C) or spread on their underlying neighbors ($n=3$) [18].

Lisa Manning is one the first to have proposed a quantitative analytic model to evaluate the tension of a tissue as function of the cortical tension and adhesion of individual cells. The model is in 2D, but should qualitatively hold in 3D. The Fig. 1.11A shows a section of cells close to the surface of an aggregate of zebrafish embryo cells, showing an approximate hexagonal organization. Manning therefore assumes this organization for the whole tissue, with however two different cases for cells at the surface, the interface of which with the cell medium shall round up because of Laplace's pressure. Two cases are observed experimentally:

- (a) When the expression of the E-cadherin adhesion molecule is down-regulated, the embryo surface displays compact cells, which do not elongate over the aggregate surface.
- (b) When the aggregate is formed with ectoderm embryonic cells, surface cells tend to elongate to spread over $n \sim 3$ underlying neighbors.

Below we will follow the calculation of tissue tension made by Manning in 2D for these two cases.

(a) Compact surface cells

Calling γ_i the line tension of each cell edge i , the total energy of the tissue is

$$\mathcal{E} = \sum_{i \text{ in}} 2\Gamma_i L_i + \sum_{i \text{ surf}} \gamma_i \ell_i \quad (1.12)$$

There are two types of interfaces. The interfaces between two cells for which $\Gamma_i = \Gamma_0 = \Gamma_a - \frac{W}{2}$, where Γ_a is the active tension of the cortex at cell-cell interfaces and W the adhesion energy per unit line. The cell-medium interfaces may have a different contractility and have no adhesion contribution, they are denoted by $\gamma_i = \gamma_s$. Cells are supposed to have a constant area. Because of this constraint surface cells are deformed $\tilde{L} \neq L$ and this deformation contributes to the tissue surface tension. In the next we introduced an effective adhesion energy $\omega = W + 2(\gamma_s - \Gamma_a)$, which includes the real adhesion and the difference of cortical tensions between the inside and surface of the tissue.

The energy of one cell inside the tissue becomes

$$\epsilon_{\text{in}} = 6L \left(\Gamma_a - \frac{W}{2} \right) = 6L \left(\gamma_s - \frac{\omega}{2} \right) \quad (1.13)$$

and for a cell at the tissue surface

$$\epsilon_{\text{surf}} = 2 \left(L + \tilde{L} \right) \left(\gamma_s - \frac{\omega}{2} \right) + \ell \gamma_s \quad (1.14)$$

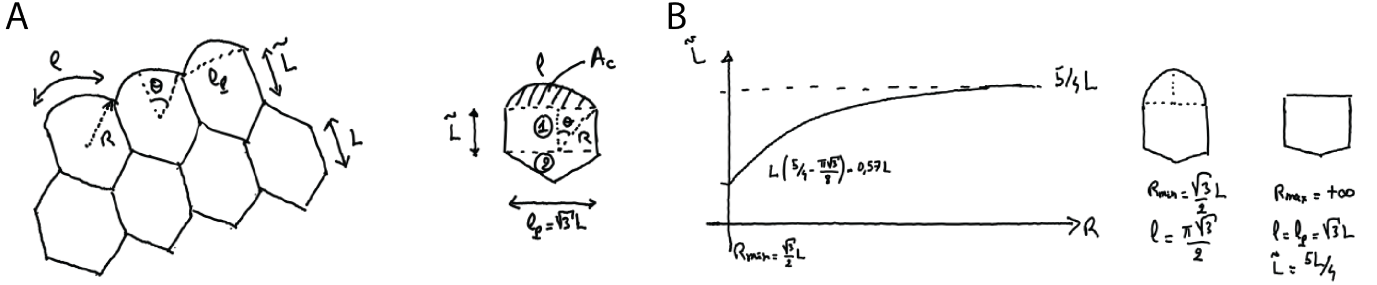


Figure 1.12: (A) Geometrical parametrization of the compact tissue configuration. (B) Plot of \tilde{L} as function the curvature radius R of outer interfaces.

The tissue (line) tension may then be defined as the difference of energy between a cell at the surface and inside the tissue, divided by the length of a cell at the surface $\ell_p = 2L \sin 2\pi/3 = \sqrt{3}L$

$$\sigma \equiv \left(\frac{\Delta \mathcal{E}}{\text{one cell}} \right) \left(\frac{\text{one cell}}{A_{\text{proj}}} \right) = \frac{\epsilon_{\text{surf}} - \epsilon_{\text{in}}}{\ell_p} = \frac{\ell \gamma_s + \left(\gamma_s - \frac{\omega}{2} \right) (2\tilde{L} - 4L)}{\sqrt{3}L} \quad (1.15)$$

Now we can use the area constraint to calculate the relation between the curvature radius of the curved edge at the border, and the lateral length of surface cells: $A = 6 \frac{L\sqrt{3}}{2} \frac{L}{2} = \frac{3\sqrt{3}}{2}L^2 = A_c + A_1 + A_2$.

We have furthermore $A_1 = \tilde{L} \ell_p = \sqrt{3}L\tilde{L}$, $A_2 = \frac{\sqrt{3}}{4}L^2$ and $A_c = R^2\theta - \frac{\ell_p}{2}R \cos \theta = R^2\theta - \frac{\sqrt{3}}{2}RL \cos \theta$, which leads to the relation

$$\tilde{L} = \frac{5}{4}L - \frac{A_c}{L\sqrt{3}} \quad (1.16)$$

and we can plot \tilde{L} as function of R as shown on Fig. 1.12

There are two limit cases:

- When the upper portion of surface cells makes an hemisphere $R = R_{\text{min}} = \frac{\sqrt{3}}{2}L$, then $\tilde{L} = L \left(\frac{5}{4} - \frac{\pi\sqrt{3}}{8} \right)$ and $\ell = \frac{\pi\sqrt{3}}{2}$. The tissue tension becomes $\sigma = \frac{\pi}{2}\gamma_s - \left(\gamma_s - \frac{\omega}{2} \right) 1.64$
- When the upper portion of surface cells is flat $R = R_{\text{max}} = +\infty$, then $\ell = \ell_p = \sqrt{3}L$ and $\tilde{L} = \frac{5}{4}L$. The tissue tension becomes $\sigma = \gamma_s - \frac{\sqrt{3}}{2} \left(\gamma_s - \frac{\omega}{2} \right) \geq 0$.

For a given fixed value of $\frac{\omega}{\gamma_s}$, the \tilde{L} will be the one that minimizes the surface energy (force balance). Manning has solved numerically this equation and can hence calculate the surface tension for any value of the ratio $\frac{\omega}{\gamma_s}$, as shown on Fig. 1.13.

If $\frac{\omega}{\gamma_s} \geq 2$, the effective adhesion energy dominates over the tension at the surface and surface cells will spread over more than a single inside cell. This is the case discussed below in the paragraph (b). If $\frac{\omega}{\gamma_s}$ becomes too small, then the tissue surface tension becomes negative. The value $\sigma = 0$ is obtained for $R = R_{\text{min}}$ and $\frac{\omega}{\gamma_s} = 0.186$. Below this value the tissue is not confluent anymore (not fully compacted).

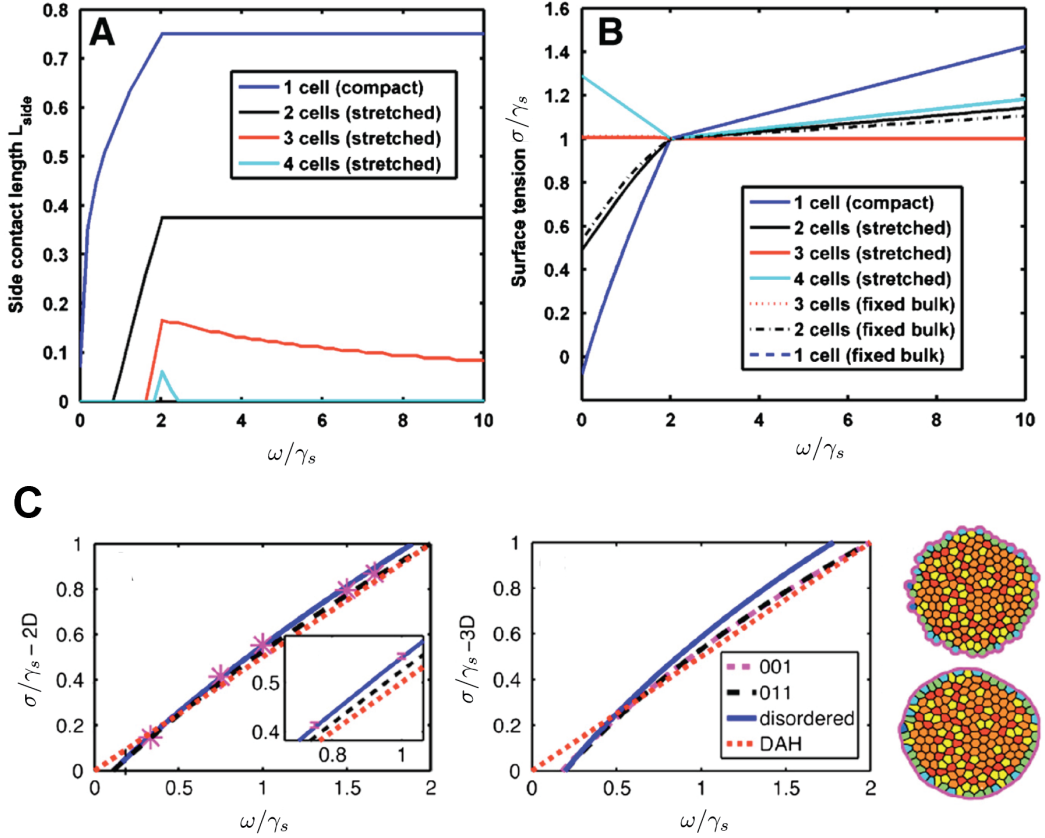


Figure 1.13: (A) Contact length \tilde{L} of surface cells as function of the ratio of adhesion and surface cortical tension ω/γ_s (B) Plot of the normalized tissue tension σ/γ_s as function the curvature radius R of outer interfaces. (C) Plot of the tissue surface tension σ in units γ_s as function of ω/γ_s . The dashed black line is the analytic calculation for ordered packing, the blue line for a disordered aggregate. The dotted red line is $\sigma = \omega/2$ corresponding to the DAH. On the right are examples of minimum energy aggregate simulations in 2D for $\omega/\gamma_s \sim 0.33$ and $\omega/\gamma_s \sim 1.667$ [18]

(b) Elongated surface cells

For strong adhesion $\frac{\omega}{\gamma_s} \geq 2$, the surface cells will spread over several underlying cells from the previous layer. The tissue surface tension becomes simply γ_s and a surface cell will elongate as much as possible to minimize area. A regulation mechanism is then necessary to limit spreading, for example the availability of cadherin molecules. In her work, Manning introduces in 2D a term proportional to the squared perimeter for each cell, that limits the spreading. There could also be deformations of internal cells as a response to surface cells spreading, but numerical simulations predict that they remain very small and may therefore not contribute much to tissue tension.

Conclusion

Generalizing her results to 3 dimensions using numerical simulations, L. Manning obtains qualitatively similar results and she finds (see Fig. 1.13C) that Steinberg's hypothesis is relatively well verified theoretically for $\omega < 2\gamma_s$ (with an effective adhesion strength ω per unit surface instead of the pure adhesion energy W). At stronger adhesion strengths, the tissue surface tension $\sigma \sim \gamma_s$ and surface cells become much more elongated.

Chapter 2

Vertex models of tissues

Epithelia form one of the four basic animal tissue along with connective, muscle and nervous tissues and are omnipresent in animal organs. It generally consists in a thin continuous and tightly compacted layer of cells, which forms the outer or inner layer of many organs and cavities, such as the epidermis in the skin. Epithelial tissues can be formed of a single layer or by two or more stratified cell layers, where cells generally adopt three major types of shapes in 3 dimensions: squamous, columnar and cuboidal (see Fig 2.1f). In this chapter, we will focus on epithelial monolayers from a mechanical perspective, through the lens of so-called *vertex models*, which are discrete and simple models of cell shape and mechanics parametrized by vertices.

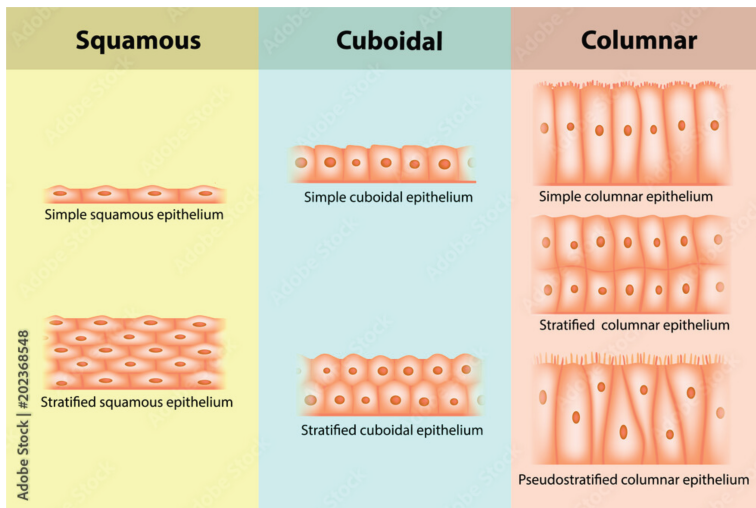


Figure 2.1: The three main types of epithelial cell organization: squamous, cuboidal and columnar. The epithelial tissue can be made of a monolayer or by several stratified (or pseudo-stratified) layers of cells.

2.1 2D vertex models of epithelial tissues

The figure 2.2 shows a monolayer epithelium, the wing of the drosophila, imaged from above (*apical* surface) using a confocal microscope, with fluorescently labeled cell membranes. Cells in monolayers adopt very commonly regular polygonal shapes, which motivates their discrete modeling as polygons in 2D or polyhedra in 3D. In Fig. 2.3, we show that the polygonal organization of epithelial monolayer does not depend on the tissue type (wing vs. notum of the Drosophila), and we illustrate the 3D structure of an epithelium with a side-view of a suspended monolayer of MDCK cells [19].

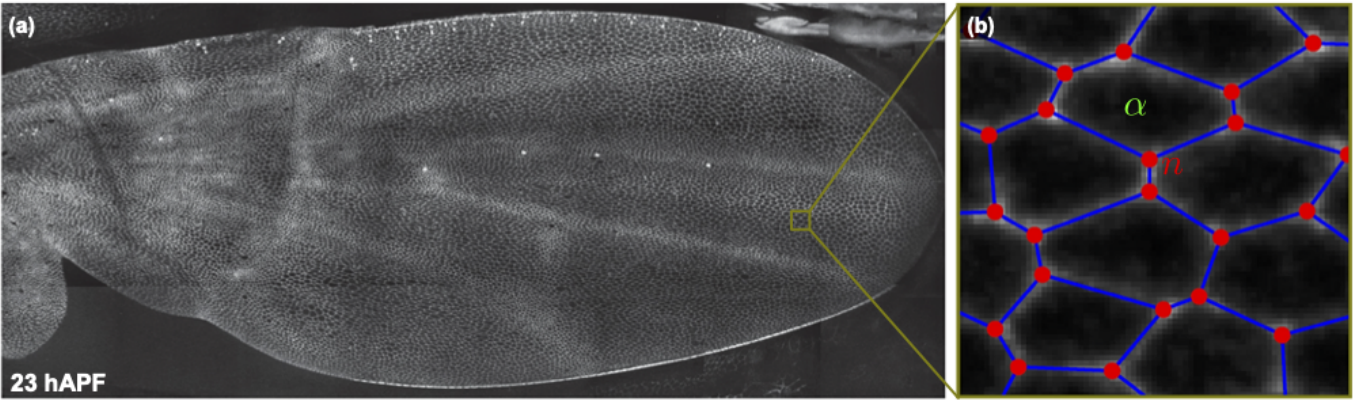


Figure 2.2: Microscopy image of a Drosophila wing and corresponding 2D polygonal representation [20]

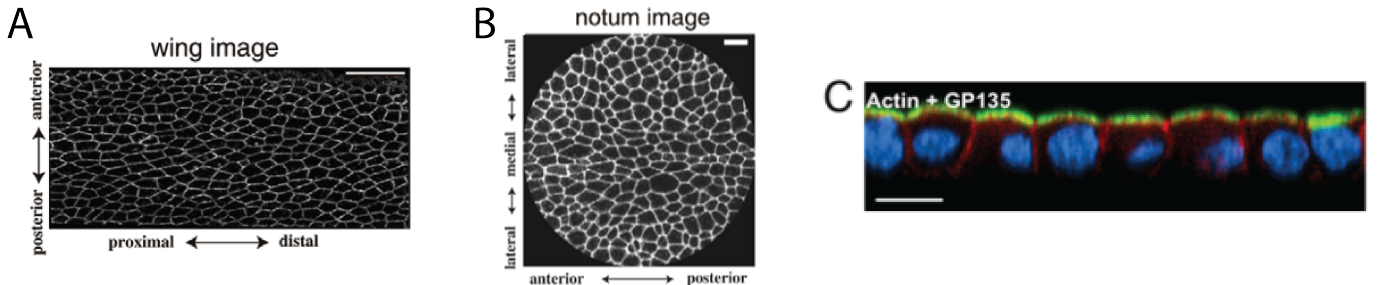


Figure 2.3: Microscopy images of a piece of the Drosophila wing (A), of the Drosophila notum (B) [21] and side-view of a suspended monolayer of MDCK cells [19]

2.1.1 Topology

Euler relation

We first establish a few mathematical relations for a surface paved by polygons. This paving is modeled

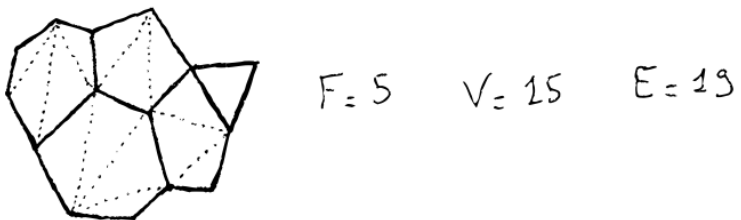


Figure 2.4

as a graph of F polygons (or faces), V vertices and E edges. On the example below on Fig. 2.4, we have specifically $F = 5$, $V = 15$ and $E = 19$. Euler found a topological relationship between these numbers

$$F + V - E = 1 \tag{2.1}$$

The demonstration may be done graphically: by adding an edge in a polygon (dashed lines on Fig. 2.4) to form a triangle, one doesn't change $F + V - E$ because one adds one edge and one face. Doing so, one can replace the polygonal paving into a triangular mesh, keeping $F + V - E$ constant. Similarly, if one triangle at the border of the paving is removed, $F + V - E$ remains constant. At the end, one has one triangle left, for which the relation $F + V - E = 1$ becomes obvious.

Topological transitions

In 2D epithelial tissues, we generally find only 3-fold junctions: each vertex has exactly 3 edges. This

property is well known in foams, where 4-fold junctions or junctions of higher degrees are unstable and will spontaneously evolve toward 3-fold junctions. This topological transition is generally called a T1-transition, which is schematized on Fig. 2.5. Another classical topological transition happening in epithelial tissues is the T2-transition, which corresponds to the disparition of a cell (because of cell death or cell extrusion) and reformation of a new 3-fold junction instead.

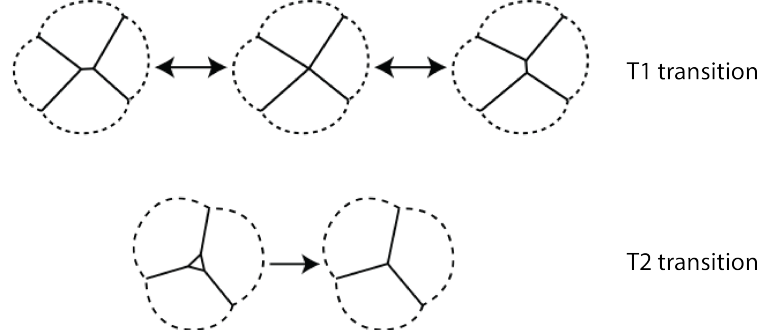


Figure 2.5: T1 and T2 topological transitions

Hexagonal packing

Epithelial tissues adopt often cell packing which are close to hexagonal networks. This fact may be understood through a simple mean-field argument. Because of the presence of 3-fold junctions only, the number of vertices and edges are related to each others as follows $3V = 2E$. The mean number of edges in a polygon is $\langle n \rangle \equiv \frac{2E}{F} = \frac{3V}{F}$ (each edge is shared between 2 polygons). From the Euler relation, we have furthermore $1 + \frac{V}{F} - \frac{E}{F} = \frac{1}{F}$, which leads to $\langle n \rangle (\frac{1}{3} - \frac{1}{2}) + 1 = \frac{1}{F}$. Taking the limit of a large tissue $F \rightarrow +\infty$, we obtain therefore $\langle n \rangle = 6$.

The mean polygon for large tissues is therefore akin a to an hexagon with 6 edges. If there exists polygons of less than 6 edges, then the tissue will also necessarily have polygons of more than 6 edges as well.

2.1.2 2D vertex model

The cell elasticity is dominated by the cortical contractility, but different interfaces and junctions may have different contributions to tension. Lateral surfaces (cell-cell contact) are the sum of adhesive and cortical contributions. The apical and basal (which adheres to the basement membrane) surfaces are both under tension, but each the apical side is furthermore equipped with an actomyosin belt, which follows cell junctions and is highly contractile, creating an additional line tension. We will describe the mechanics of the epithelial tissue using a polygonal paving of its apical surface. The contribution of lateral surface and basal surface are essentially neglected (see Fig 2.6). In 2-dimensions, the cell elasticity depends on the face and tensions are line tensions located at edges.

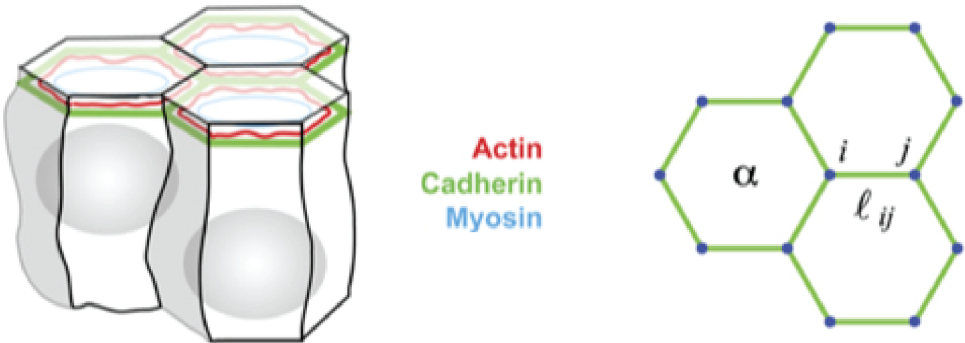


Figure 2.6: Schematics of the epithelium and corresponding 2D vertex model

Following the notations in the original publication [22], each cell is defined by an index α , each vertex by an index i and each edge by a pair of indices $< i, j >$. The force may be derived from an effective energy that reads

$$\mathcal{E} = \sum_{\alpha} \frac{\kappa_{\alpha}}{2} (A_{\alpha} - A_{\alpha}^0)^2 + \sum_{<i,j>} \Lambda_{ij} \ell_{ij} + \frac{1}{2} \sum_{\alpha} \Gamma_{\alpha} P_{\alpha}^2 \quad (2.2)$$

The first term supposes that for each cell α there is a surface elasticity associated to the constant κ_{α} , which tends to bring the current area A_{α} back to its preferred value A_{α}^0 . This term is associated to the apical tension, but may also somehow account for the effective elastic response of a cell in 3D, which has a preferred shape dictated by apical, basal and lateral tensions and the constraint of volume conservation.

Λ_{ij} is the (line) tension associated to an edge $< i, j >$ and the last term accounts for the possible variation of tension with the cell shape, here via the square of its perimeter P_{α} . The effective tension will be different at each edge because of this term.

Ground states of a single cell

Here we follow in particular [23]. In the next, we suppose an homogeneous tissue, such that $\kappa_{\alpha} = \kappa$, $\Lambda_{ij} = \Lambda$ and $\Gamma_{\alpha} = \Gamma$. The tissue energy reduces then to a simple sum on each cell

$$\mathcal{E} = \sum_{\alpha} \frac{\kappa}{2} (A_{\alpha} - A_0)^2 + \frac{\Lambda}{2} P_{\alpha} + \frac{\Gamma}{2} P_{\alpha}^2 \quad (2.3)$$

The energy is renormalized to work with dimensionless parameters. We choose as characteristic length in the tissue $\sqrt{A_0}$, such that $A_{\alpha} = A_0 a_{\alpha}$, $P_{\alpha} = \sqrt{A_0} p$, and we define $\bar{\Lambda} = \frac{\Lambda}{\kappa A_0^{3/2}}$, $\bar{\Gamma} = \frac{\Gamma}{A_0 \kappa}$, $p_0 = -\frac{\Lambda}{2\Gamma}$ and $e_0 = -\frac{\bar{\Lambda}^2}{8\Gamma}$, such that the dimensionless energy reads

$$\bar{\mathcal{E}} \equiv \frac{\mathcal{E}}{\kappa A_0^2} = \sum_{\alpha} \left\{ \frac{(a_{\alpha} - 1)^2}{2} + \frac{\bar{\Gamma}}{2} (p_{\alpha} - p_0)^2 + e_0 \right\} \quad (2.4)$$

The system is therefore controlled by 3 dimensionless parameters $\bar{\Gamma}$, p_0 and e_0 .

We first study the configuration of a single, cell. Its dimensionless energy is simply $e = \frac{1}{2}(a - 1)^2 + \frac{\bar{\Gamma}}{2}(p - p_0)^2 + e_0$. Dilating the cell by a factor α , we obtain

$$e(\alpha) = \frac{1}{2} (\alpha^2 a - 1)^2 + \frac{\bar{\Gamma}}{2} (\alpha p - p_0)^2 + e_0$$

The energy is minimal for a non-dilated cell if and only if $\frac{\partial e}{\partial \alpha} \Big|_{\alpha=1} = 0$, which gives

$$2a(a - 1) + \bar{\Gamma}p(p - p_0) = 0 \quad (2.5)$$

One can distinguish four possible cases:

- **$a = 1$ and $p = p_0$** : this is the absolute minimum of the energy $e = e_0$, at which both area and perimeter take their preferred values. More details are given below
- **$a > 1$ and $p < p_0$** : such cell is unstable with respect to shear, because $\frac{\partial e}{\partial p} \Big|_a = \bar{\Gamma}(p - p_0) < 0$ and it is always possible to decrease the energy by increasing the perimeter at fixed area.
- **$a < 1$ and $p > p_0$** such cell is stable with respect to shear, because $\frac{\partial e}{\partial p} \Big|_a = \bar{\Gamma}(p - p_0) > 0$, so at fixed area, one can decrease the energy by lowering the perimeter.

- $a = 0$ and $p = 0$: this is a collapsed cell, for which the energy is $e_c = e_0 + \frac{\bar{\Gamma}}{2} p_0^2 + \frac{1}{2} = \frac{1}{2}$.

The case $a = 1$ and $p = p_0$ gives an absolute minimum of the energy but it can be accessed only for certain values of the perimeter p_0 . For an area $a = 1$, the minimal perimeter is the one of a regular polygon with n sides¹: $p_0 = -\frac{\bar{\Lambda}}{2\bar{\Gamma}} \geq (4n \tan \frac{\pi}{n})^{\frac{1}{2}}$, which gives

$$\bar{\Lambda} \leq \bar{\Lambda}_n \equiv -4\bar{\Gamma} \left(n \tan \frac{\pi}{n} \right)^{1/2} \quad (2.6)$$

For $n = 3, 4, 5, 6, \dots$, we can therefore define threshold values of $\bar{\Lambda}$ such that $\bar{\Lambda}_3 < \bar{\Lambda}_4 < \bar{\Lambda}_5 < \bar{\Lambda}_6 = -\bar{\Gamma} 2^{5/2} 3^{1/4} \dots < -4\bar{\Gamma}$, such that if $\bar{\Lambda} > \bar{\Lambda}_n$, only polygons of more than n sides (strictly) are at a minimum of energy. For instance, for $\bar{\Lambda} \geq \bar{\Lambda}_5$, the (absolute) minimum is reached for (irregular) hexagons and polygons of more than 6 sides.

The case $a < 1$ and $p > p_0$: if $p > p_0$, at fixed area, one can decrease the energy by lowering the perimeter. This case always leads either to regular polygons or a collapsed cell ($a = 0, p = 0$). A regular polygon has a smaller perimeter than any irregular n -sided polygon with the same area. Thus if $p > 0$, the optimal cell shape is a regular n -sided polygon. For a regular polygon, the area is given by $a = \frac{\cot(\pi/n)}{4n} p^2 \equiv c_n p^2$. The minimum of the energy is obtained for this regular polygon if the condition Eq. 2.5 is verified, which gives

$$2c_n p^2 (c_n p^2 - 1) + \bar{\Gamma} p(p - p_0) = 2c_n p^2 (c_n p^2 - 1) + \bar{\Gamma} p^2 + \bar{\Lambda} p = 0 \quad (2.7)$$

This minimum is locally stable if and only if its energy is less than the one of a collapsed cell $e(p) \leq \frac{1}{2}$.

A necessary condition for polygonal collapse is given by $e(p) > \frac{1}{2}$, which combined with the equation for stability Eq. 2.7 determines the transition through the two quantities $\bar{\Gamma}$ and p and leads to two cases [23]

- If $\bar{\Gamma} \geq 2c_n$, the only solution is $p = \bar{\Lambda} = 0$, which corresponds to a collapsed cell.
- If $\bar{\Gamma} < 2c_n$, the collapse it attained for $\bar{\Lambda} > \bar{\Lambda}_c = \frac{2}{c} \left(\frac{2c-\bar{\Gamma}}{3} \right)^{3/2}$ where $p = \frac{3}{c_n} (2c_n - \bar{\Gamma})^{1/2}$.

For hexagons, for which $c_6 = \frac{1}{8\sqrt{3}}$. If $\bar{\Lambda} = \bar{\Lambda}_6 = -2^{5/2} 3^{1/4} \bar{\Gamma}$, the equation (2.7) is verified for $a = 1$ and $p = 3^{1/4} 2^{3/2}$. If $\bar{\Lambda} > \bar{\Lambda}_6$ at $\bar{\Gamma}$ fixed, then the area and perimeter of hexagons is decreasing with $\bar{\Lambda}$. This can lead to collapsed cells (unstable tissue) and regular hexagons of area less than 1. The transition to collapse from hexagonal cells is therefore given by the two cases (as summarized in the Table Fig.2.7A):

- If $\bar{\Gamma} \geq \frac{\sqrt{3}}{12}$, the only solution is $p = \bar{\Lambda} = 0$, which corresponds to a collapsed cell.
- If $\bar{\Gamma} < \frac{\sqrt{3}}{12}$, the collapse it attained for $\bar{\Lambda} > \bar{\Lambda}_c = 2 \cdot 3^{-5/2} (\sqrt{3} - 12\bar{\Gamma})^{3/2}$

Ground states of a single cell

Numerically, Staple et al. [23] are recovering for a tissue a certain number of the theoretical results obtained for a cell above and a few new configurations that combine several cell topologies.

As shown on Fig. 2.7B for $\bar{\Lambda} \leq \bar{\Lambda}_6$ (solid line), the tissue adopts a fundamental state, where the energy is at the absolute minimum ($a = 1$ and $p = p_0$), but where there exists many degenerate cases with irregular polygons of with more than 3 sides, that corresponding to soft modes of deformation (i.e. modes of deformations of the tissue that do not cost any energy). The degeneracy decreases as $\bar{\Lambda} \geq \bar{\Lambda}_n$ with $3 \geq n \geq 6$, as the n -sided polygons become impossible. Above $\bar{\Lambda}_6$, only polygons of more than 6 sides could be in the fundamental state, but that would not yield the mean side number $\langle n \rangle = 6$ predicted above. Therefore, the tissue adopts rather a regular and periodic hexagonal pattern, which does not correspond to the absolute

¹For a regular polygon of degree n , we have $\tan \frac{\pi}{n} = \frac{\ell}{h}$, where ℓ is the side length and h the apothem (shortest distance from the center to one side). We deduce the area $a = n(h \frac{\ell}{2}) = n \frac{\ell^2}{4} (\tan \frac{\pi}{n})^{-1}$, and the perimeter $p = n\ell = (4an \tan \frac{\pi}{n})^{1/2}$ as function of the area.

A

Parameter values		Ground state (identical cells)
$\bar{\Lambda} < -2^{5/2}3^{1/4}\bar{\Gamma}$	-	irregular polygons ($a = 1, p = p_0$)
$-2^{5/2}3^{1/4}\bar{\Gamma} \leq \bar{\Lambda} < 2 \cdot 3^{-5/2}(\sqrt{3} - 12\bar{\Gamma})^{3/2}$	$\bar{\Gamma} < \sqrt{3}/12$	hexagonal lattice }
$-2^{5/2}3^{1/4}\bar{\Gamma} \leq \bar{\Lambda} < 0$	$\bar{\Gamma} \geq \sqrt{3}/12$	
$\bar{\Lambda} \geq 2 \cdot 3^{-5/2}(\sqrt{3} - 12\bar{\Gamma})^{3/2}$	$\bar{\Gamma} < \sqrt{3}/12$	collapsed lattice ($a = 0, p = 0$) }
$\bar{\Lambda} \geq 0$	$\bar{\Gamma} \geq \sqrt{3}/12$	

B

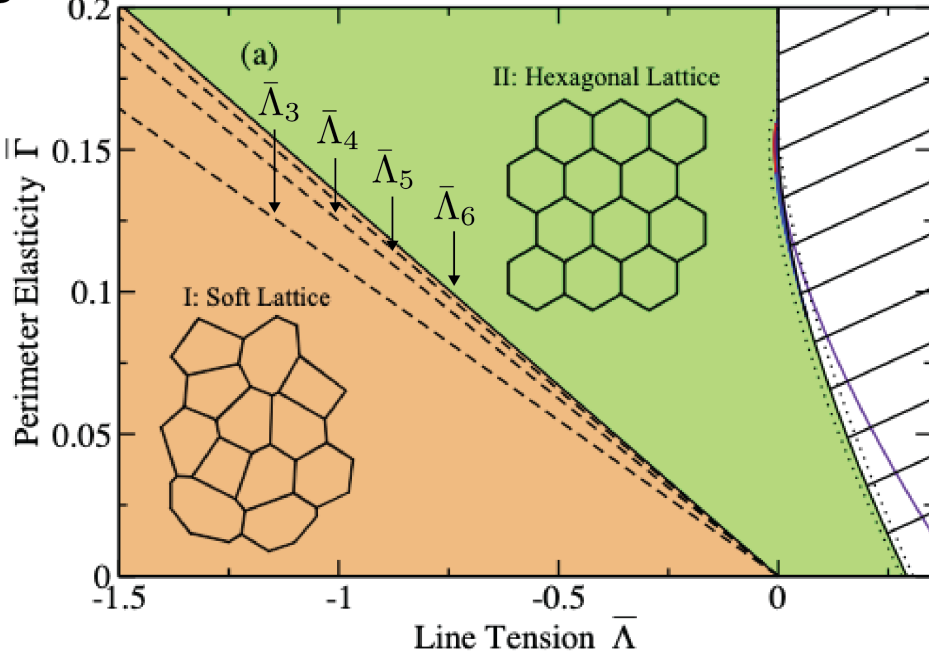


Figure 2.7: Ground state for the 2D vertex model [23]. (A) Table of the different transition boundaries between the different ground states depending on $\bar{\Lambda}$ and $\bar{\Gamma}$. (B) Numerical phase diagram of the ground state for the 2D vertex model as function of $\bar{\Gamma}$ and $\bar{\Lambda}$ with the corresponding transition boundaries predicted theoretically.

minimal state of energy $\mathcal{E} = N_{\text{cell}}e_0$. The new fundamental state corresponds to hexagons with $a < 1$ and $p > p_0$. This structure remains stable if cells don't collapse. The conditions of collapse were predicted for a single cell above for the particular case of an hexagon, and are reported in the Table Fig. 2.7A.

Numerically, the authors find that the regular hexagonal pattern is the only fundamental state for $\bar{\Lambda} \geq \bar{\Lambda}_6$, except for two very small regions depicted in more details on Fig. 2.8. Two regions with two different types of cells organized in a periodic manner can have a lower energy than the hexagonal arrangement and are represented in red and blue.

Comparison to experiments

In Farhadifar et al. [22], the authors compare the shape properties of the 2D vertex model with the cell packing observed in imaginal disk of the Drosophila wing. The authors add growth and division (proliferation) and allow for topological transitions (T1 and T2 transitions, see Fig. 2.5 and study the statistical properties of stationnary states. They systematically vary $\bar{\Gamma}$ and $\bar{\Lambda}$ to get the best fit to measured values of the distribution of polygons and their mean area (see Fig. 2.9. They also use laser ablation experiments to directly compare the relative area and bon length change depending on the values of $\bar{\Gamma}$ and $\bar{\Lambda}$.

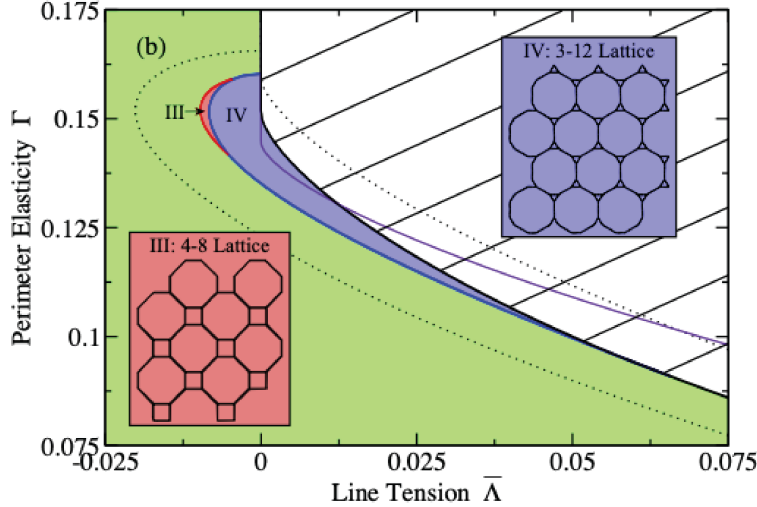


Figure 2.8: Ground state for the 2D vertex model - Possible non-hexagonal patterns with two cell types for $\bar{\Lambda} \geq \bar{\Lambda}_6$ [23].

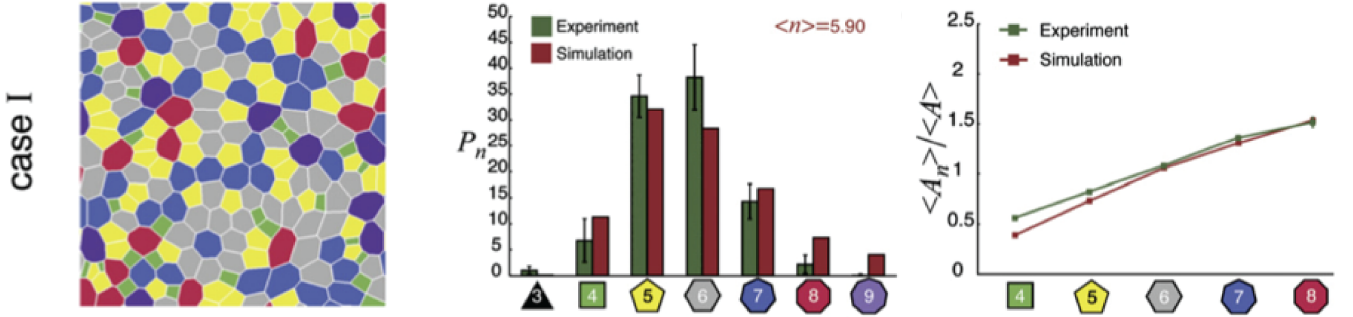


Figure 2.9: Schematics of the epithelium and corresponding 2D vertex model [22].

2.2 3D vertex models

To better account for the 3D structure of cells, several 3D vertex models have been proposed in the last decades, relying mostly on numerical implementations. Here we will focus on a model that was proposed by Hannezo et al. [24], because it remains relatively easy to describe analytically.

2.2.1 Epithelial 3D vertex model

Here, we follow the model proposed by Hannezo et al. [24].

To simplify we consider a monolayer of cells, that are all **identical**, and whose **apical surface remains hexagonal**. The basal surface has therefore also an hexagonal geometry and lateral surfaces are parallelograms. We note h the height of a cell and r the radius of the circle circumscribed to the hexagon. A cell is defined as columnar when $\frac{h}{r} \gg 1$, squamous when $\frac{h}{r} \ll 1$ and cuboidal when $\frac{h}{r} \sim 1$.

The apical area is $A_a = r^2 \frac{3^{3/2}}{2}$, and the total lateral surface area is $A_L = 6rh$. The volume of the cell is simply $V = Ah$.

Exactly like for the 2D vertex model, we write an energy that accounts for the tensions (and adhesion) at each interface, the minimization of which defining the mechanical equilibrium. For a single cell it reads

$$e = \gamma_L A_L + \gamma_b A_b + \gamma_a A_a + \Lambda P + \frac{K}{2} \frac{(V - V_0)^2}{V_0} \quad (2.8)$$

where γ_L , γ_a , γ_b are surface tensions of respectively the lateral, apical and basal surfaces, Λ is the apical line

tension, multiplied by the apical perimeter P and K measures the cell compressibility, which shall bring the volume V of the cell back to its target value V_0 . This compression modulus is supposed high in the next, such that $V \sim V_0$. $\gamma_L, \gamma_a, \gamma_b$ have a positive contribution from the actomyosin contractility, but γ_L and γ_b also have a negative contribution coming from cell-cell adhesion for lateral surfaces and from the adhesion to the basal membrane for the basal surface. In principle, they may therefore become negative as well.

Flat epithelial monolayers

In the next, to simplify we define $\gamma = \gamma_a + \gamma_b$, as the monolayer is supposed to remain flat in this paragraph. We further ignore numerical prefactors, which simply renormalize the tensions. The energy for a cell reads then simply

$$e = \gamma r^2 + \Lambda r + \gamma_L \frac{V_0}{r} \quad (2.9)$$

where we have used the constraint of volume conservation to express $h = \frac{V_0}{A} \sim \frac{V_0}{r^2}$.

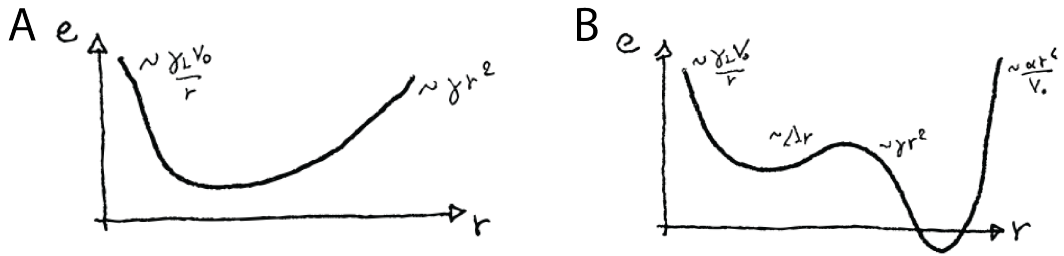


Figure 2.10: Sketch of the plot of the cell energy for a flat 3D vertex model (A) If $\gamma > 0$, there is a single minimum. (B) if $\gamma < 0$, there can be two minima, adding a limit to compressibility with a new term $\frac{\alpha}{h^2} \sim \frac{\alpha r^4}{V_0}$.

If $\gamma > 0$, there is a single minimum of the energy, given by the derivative of e with r :

$$2\gamma r + \Lambda - \gamma_L \frac{V_0}{r^2}$$

We sketch the plot of the energy on Fig. 2.10A and we can distinguish two limit cases

- If Λ is high enough, then r will be small and the equation above reduces to $\Lambda - \gamma_L \frac{V_0}{r^2} \sim 0$, which gives $r = \left(\frac{V_0 \gamma_L}{\Lambda} \right)^{1/2}$ and $h = \frac{\Lambda}{\gamma_L}$.
- If Λ is small enough, then it is negligible and the equation above reduces to $2\gamma r^2 - \gamma_L \frac{V_0}{r^2} = 0$, which leads to $r = \left(\frac{\gamma_L V_0}{2\gamma} \right)^{1/3}$

One can see that r increases if γ and/or Λ decreases and if γ_L increases: we switch continuously from columnar cells (very elongated vertically) to squamous cells (very flat).

If $\gamma < 0$, the energy may be non-monotonous as sketched on Fig. 2.10B. The absolute minimum is for $r \rightarrow +\infty$, but the cell cannot collapse fully because there is incompressible material within. To account for this effect, a new term is added to the energy in the form $e_{\text{com}} = \frac{\alpha}{h^2} \sim \frac{\alpha r^4}{V_0}$. This creates a second possible minimum, with a possible discontinuous transition between the two minima².

²By adding this additional term, one can write the energy for a cell $e = \gamma A + \frac{\alpha}{V_0^2} A^2 + (\Lambda + \gamma_L h) P$. If one considers Λ much larger than $\gamma_L h$, which means that we ignore the lateral tension, we recover almost the expression used by Farhadifar's et al [22] for the 2D vertex model. The term $\frac{\Gamma P^2}{2}$, which comes from the variation of the tension with the perimeter P is however missing.

Tissue under tension

The tension of the tissue may be defined as the derivative of the energy with respect to the area. At the level of a single cell, it reads therefore

$$\Gamma = \frac{\partial e}{\partial A} = \frac{1}{2r} \frac{\partial e}{\partial r} = \gamma + \frac{\Lambda}{2r} - \frac{\gamma_L V_0}{2r^3} \quad (2.10)$$

At mechanical equilibrium, (no tension) we should have $\Gamma = 0$. The plot of the tissue tension is sketched on Fig. 2.11

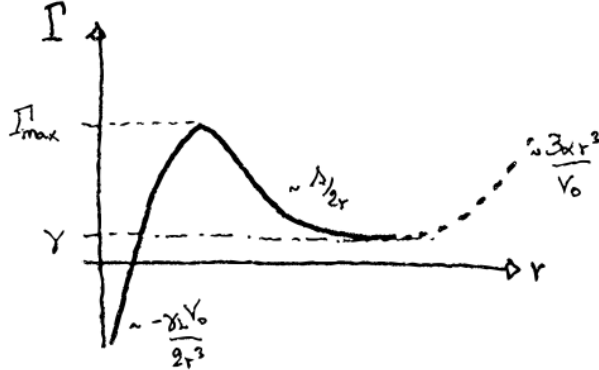


Figure 2.11: Sketch of the plot of the tissue tension for a flat 3D vertex model. The dotted line is the continuation of the tissue tension if the term $\frac{\alpha}{h^2} \sim \frac{\alpha r^4}{V_0}$ is added to the energy.

We see that the tension reaches a maximum $\Gamma_{\max} = \gamma_L + \frac{\Lambda^{3/2}}{2\sqrt{3}\gamma_L V_0} \left(1 - \frac{\gamma_L}{6}\right)$, which is obtained for $r = \left(\frac{2\gamma_L V_0}{\Lambda}\right)^{1/2}$. As $r \rightarrow +\infty$, the tissue tension approaches γ_L .

For $\Gamma > \Gamma_{\max}$ then the tissue is unstable and there is no solution other than $h \rightarrow 0$, unless the additional term $\frac{\alpha}{h^2} \sim \frac{\alpha r^4}{V_0}$ is added. In the case of a discontinuous transition $\gamma < 0$, the tissue tension transforms columnar cells into cuboidal or squamous cells.

2.2.2 Non-epithelial 3D vertex models

3D polyhedral models

In fact, the first 3D vertex models were proposed by Honda et al. [25]. In this paper, the authors study the flattening of a small aggregate made of polyhedral cells under the action of a centrifugal volume force. In this model, there is still a geometric constraint on cells, which are supposed to have flat interfaces, neglecting hence Laplace's pressure.

The total energy of the system is defined as

$$\mathcal{E} = \sigma \sum_{<\alpha, \beta>} A_{\alpha\beta} + \sigma_0 \sum_{<\alpha, 0>} A_{\alpha 0} + \kappa \sum_{\alpha} (V_{\alpha} - V_0)^2 + \rho \sum_{\alpha} z_{\alpha} V_{\alpha} + w_{\text{floor}} \sum_{\alpha} \frac{1}{1 + e^{az_{\alpha}}} \quad (2.11)$$

The first two terms account for the surface tension of cell-cell and cell-medium interfaces. The second term measures the compressibility of each cell, such that if κ is high, the volume V_{α} will stay close to its target value V_0 . The two last terms account for the centrifugal force, which creates a potential proportional to the cell height z_{α} and for the repulsion energy from the floor, which is maximum and equal to w_{floor} for $z_{\alpha} = 0$.

The deformation of the aggregate is solved by supposing a friction η on each vertex and by solving the overdamped equation balancing on each vertex i this friction force and the forces derived from the above

energy

$$\eta \frac{d\mathbf{r}_i}{dt} = -\nabla_i \mathcal{E} \quad (2.12)$$

The authors account for both T1 and T2 transitions in the vertex dynamics and obtain numerical results as shown on Fig.2.12

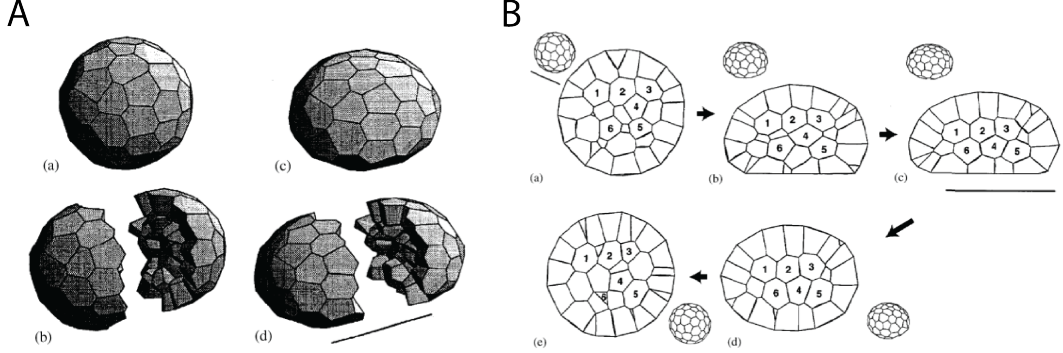


Figure 2.12: 3D polyhedral models of a cell aggregate [25]. (A) Cell aggregate modeled with polyhedral cells. (B) Section showing cell rearrangements during the flattening and recovery of the aggregate.

More recently, this approach was generalized by Okuda et al. [26], to integrate coupling between mechanics and signalling. Turing equations are solved at the multicellular scale, accounting for the transport of activator and inhibitor molecules across cells via a parameter χ , and proliferation is coupled to the activator level. Depending on parameters, this mechanochemical model can lead to various self-organized shape emergence, with budding, branching and tubulation as illustrated on Fig.2.13.

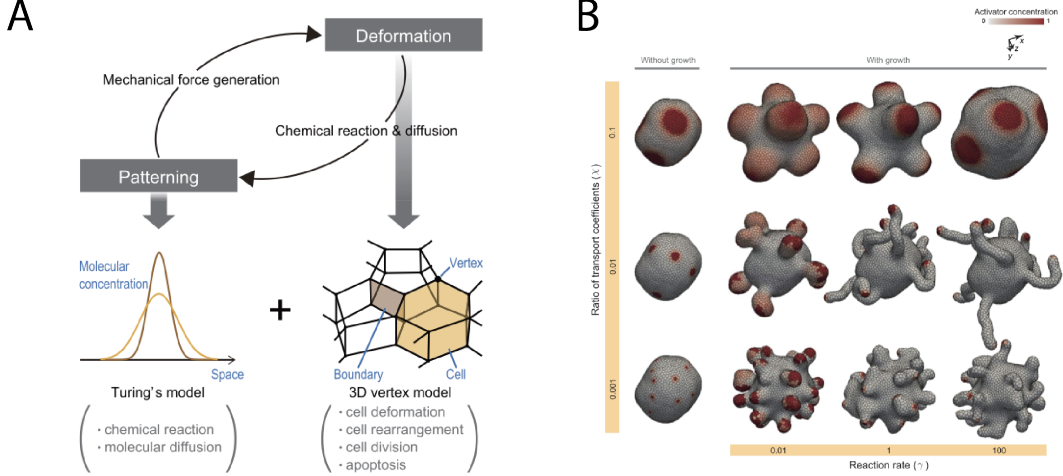


Figure 2.13: 3D mechanochemical vertex model [26]. (A) Principle of the coupling between cell mechanics and signalling. (B) Examples of self-organized shape emergence depending on a transport coefficient χ for the activator between cells, and the reaction rate γ .

Generic 3D curved vertex model

We now present a generic 3D vertex model, where the cell interfaces are not supposed flat anymore. This requires the parametrization of cell interfaces with a (triangular) mesh, as developed in [27].

Surface energy and Lagrangian function The surface energy for a set of N cells is defined as follows

$$\mathcal{E} = \sum_{\langle l,m \rangle} \gamma_{lm} A_{lm} \quad (2.13)$$

where γ_{lm} and A_{lm} are respectively the surface tension and area of the interface between regions l and m that span $\llbracket 0, N \rrbracket$. To account for volume conservation, we define a Lagrangian function from this energy, where p_l are the Lagrange multipliers (pressures) associated to the volumes V_l

$$\mathcal{L} = \mathcal{E} - \sum_{\text{cell } l \in \llbracket 1, N \rrbracket} p_l (V_l - V_l^0) \quad (2.14)$$

where V_l^0 is the target volume value of the cell l . Note that for interfaces l and m span $\llbracket 0, N \rrbracket$, where 0 refers to the external medium, while for cells l spans $\llbracket 1, N \rrbracket$.

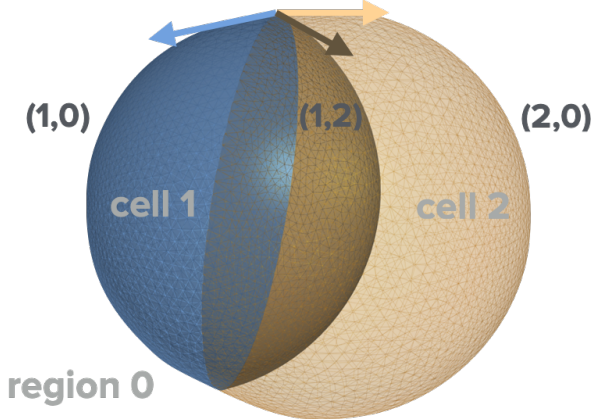


Figure 2.14: 3D curved vertex model [27]. The cells geometry is parametrized with a non-manifold triangular mesh, where each holds a doublet of integers to keep track of the regions (or cells) between which they lie.

From the Lagrangian function, one can calculate the force \mathbf{f}_k on each vertex of the mesh $\mathbf{x} \in \{\mathbf{x}_k\}_{k=1}^n$ as follows

$$\mathbf{f} = -\frac{\partial \mathcal{L}}{\partial \mathbf{x}} \quad (2.15)$$

where $\mathbf{x} = x\mathbf{e}_x + y\mathbf{e}_y + z\mathbf{e}_z$ and $\mathbf{f}_k = f^x\mathbf{e}_x + f^y\mathbf{e}_y + f^z\mathbf{e}_z$ are the decomposition of vertex position and force in the 3D Euclidean space, equipped with an orthonormal basis $(\mathbf{e}_x, \mathbf{e}_y, \mathbf{e}_z)$.

Interfacial areas and cell volumes can be easily expressed as sums on the triangles t in the mesh:

$$A_{lm} = \sum_{t \in \{lm\}} a^t, \quad V_l = \sum_{t \in l} v^t, \quad (2.16)$$

where a^t and v^t are respectively the elementary area and volume of a given triangle $t = \{\mathbf{x}_0^t, \mathbf{x}_1^t, \mathbf{x}_2^t\}$, which are given by

$$a^t = \frac{1}{2} |(\mathbf{x}_0^t - \mathbf{x}_2^t) \times (\mathbf{x}_1^t - \mathbf{x}_2^t)| \quad (2.17)$$

$$v^t = \frac{1}{6} \mathbf{x}_2^t \cdot (\mathbf{x}_0^t \times \mathbf{x}_1^t) \quad (2.18)$$

Their derivatives with respect to the vertex position $\mathbf{x} = \mathbf{x}_2^t$ may be easily calculated as

$$\frac{\partial a^t}{\partial \mathbf{x}^t} = \frac{1}{2} [\mathbf{n}^t \times (\mathbf{x}_1^t - \mathbf{x}_0^t)] \quad (2.19)$$

$$\frac{\partial v^t}{\partial \mathbf{x}^t} = \frac{1}{6} \mathbf{x}_0^t \times \mathbf{x}_1^t \quad (2.20)$$

where we have defined the normal $\mathbf{n}^t = \frac{(\mathbf{x}_0^t - \mathbf{x}_2^t) \times (\mathbf{x}_1^t - \mathbf{x}_3^t)}{2a^t}$ to the triangle t . Note that these formulae are invariant by permutation of the triplet of vertices $\{0, 1, 2\}$.

The force on a vertex \mathbf{x} defined in (2.15) may now be explicitly expressed as

$$\mathbf{f} = -\frac{\partial \mathcal{E}}{\partial \mathbf{x}} + \sum_{\text{cell1}} p_l \frac{\partial V_l}{\partial \mathbf{x}} \quad (2.21)$$

$$= -\sum_{\text{pair } \{lm\}} \frac{\gamma_{lm}}{2} \sum_{t \in \{lm\} | \mathbf{x} \in t} \mathbf{n}^t \times (\mathbf{x}_1^t - \mathbf{x}_0^t) + \sum_{\text{cell1}} p_l \sum_{t \in l | \mathbf{x} \in t} \frac{1}{6} \mathbf{x}_0^t \times \mathbf{x}_1^t \quad (2.22)$$

where we assumed without loss of generality that $\mathbf{x} = \mathbf{x}_2^t$, relying on the above invariance by permutation of derivatives formula.

Constrained optimization: projection method At mechanical equilibrium, all interfaces follow Laplace's law and each junction verifies Young-Dupré's equations. These equations may be equivalently expressed through a constrained optimization of the surface energy (2.13), where cell volumes are conserved. Using the Lagrangian function defined above in (2.14), optimality conditions are obtained when

$$\frac{\partial \mathcal{L}}{\partial \mathbf{x}} = -\mathbf{f}(\mathbf{x}) = \mathbf{0} \quad \forall \mathbf{x} \in \{\mathbf{x}_k\}_{k=1}^n \quad (2.23)$$

$$\frac{\partial \mathcal{L}}{\partial p} = 0 \quad \forall p \in \{p_l\}_{l=1}^N \iff V_l = V_l^0 \quad \forall l \quad (2.24)$$

To calculate the Lagrange multipliers $p_{l=1}^N$, which enforce the volume conservation equations (2.24), one can use a projection method. The force $\mathbf{f}_k = \mathbf{f}(\mathbf{x}_k)$ of each vertex \mathbf{x}_k is projected onto a subspace that is orthogonal to the space of cell volumes variations

$$0 = \sum_{k=1}^n \mathbf{f}_k \cdot \frac{\partial V_l}{\partial \mathbf{x}_k} \quad \forall l \in \llbracket 1, N \rrbracket \quad (2.25)$$

This leads to a linear system of equations for p_l

$$\forall l \in \llbracket 1, N \rrbracket \quad \sum_{m=1}^N p_m \sum_{k=1}^n \left(\frac{\partial V_m}{\partial \mathbf{x}_k} \cdot \frac{\partial V_l}{\partial \mathbf{x}_k} \right) = \sum_{k=1}^n \left(\frac{\partial \mathcal{E}}{\partial \mathbf{x}_k} \cdot \frac{\partial V_l}{\partial \mathbf{x}_k} \right) \quad (2.26)$$

that may be rewritten in a condensed form $\underline{\mathbf{A}} \cdot \mathbf{p} = \mathbf{b}$, where $\mathbf{p} \equiv (p_1, p_2, \dots, p_N)$ is a vector of size N collecting the unknown pressures, $\mathbf{b} \equiv \left(\sum_k \left(\frac{\partial \mathcal{E}}{\partial \mathbf{x}_k} \cdot \frac{\partial V_1}{\partial \mathbf{x}_k} \right), \sum_k \left(\frac{\partial \mathcal{E}}{\partial \mathbf{x}_k} \cdot \frac{\partial V_2}{\partial \mathbf{x}_k} \right), \dots, \sum_k \left(\frac{\partial \mathcal{E}}{\partial \mathbf{x}_k} \cdot \frac{\partial V_N}{\partial \mathbf{x}_k} \right) \right)$ is the vector of constants and $\underline{\mathbf{A}}$ is the matrix of coefficients defined by

$$A_{lm} = \sum_k \left(\frac{\partial V_m}{\partial \mathbf{x}_k} \cdot \frac{\partial V_l}{\partial \mathbf{x}_k} \right) \quad \forall l, m \in \llbracket 1, N \rrbracket \quad (2.27)$$

which is a symmetric positive definite and therefore invertible matrix. This linear system of N equations may be solved using a Newton's method [28].

To find the mechanical equilibrium, one needs to solve the equation (2.23): $\forall \mathbf{x}, \mathbf{f}(\mathbf{x}) = 0$. To do so, one can use an iterative method, for instance the conjugate gradient, whereby the position $\mathbf{x}(t)$ of each vertex at time t is updated iteratively along a new search direction \mathbf{D}_{t+1} that is conjugate to the one at previous time step \mathbf{D}_t [28].

At each iteration, the cell pressures are recalculated using the projection method.

The constrained optimization method is applied to a non-manifold multimaterial mesh. The identity of each interface separating cells i and j is tracked over its evolution by a label of integers (i, j) that is stored in each triangle of the interface. To maintain numerical precision, the triangular mesh is furthermore allowed to vary the number of vertices, edges and faces over its evolution (remeshing), and to perform topological transitions: T1 (neighbor exchange), T2 (region collapse) and merging (new contact). Note that, in contrast to classical vertex models where cell-cell boundaries are assumed to remain flat, this generic vertex model does not impose any prior constraints on cell shapes. Its precision to represent smooth and continuous interfaces is only limited by the user-defined resolution of the triangular mesh.

Chapter 3

Continuous models of tissues - dissipation and nematic order

In this chapter, that will be the subject of two lessons, we will discuss continuous descriptions of tissues. During embryonic development or organ formation, morphogenesis relies on the collective motion of thousands of cells that deform, rearrange, divide,, die and flow to establish the shape of a tissue. At large scales, one may expect the emergence of collective behaviors and features that are independent of the microscopic details of cellular organization. Continuum approaches require the existence of an intermediate length scale, larger than a typical cell size, but smaller than the spatial extension of the tissue.

3.1 Preliminary: continuum mechanics, a minimal introduction

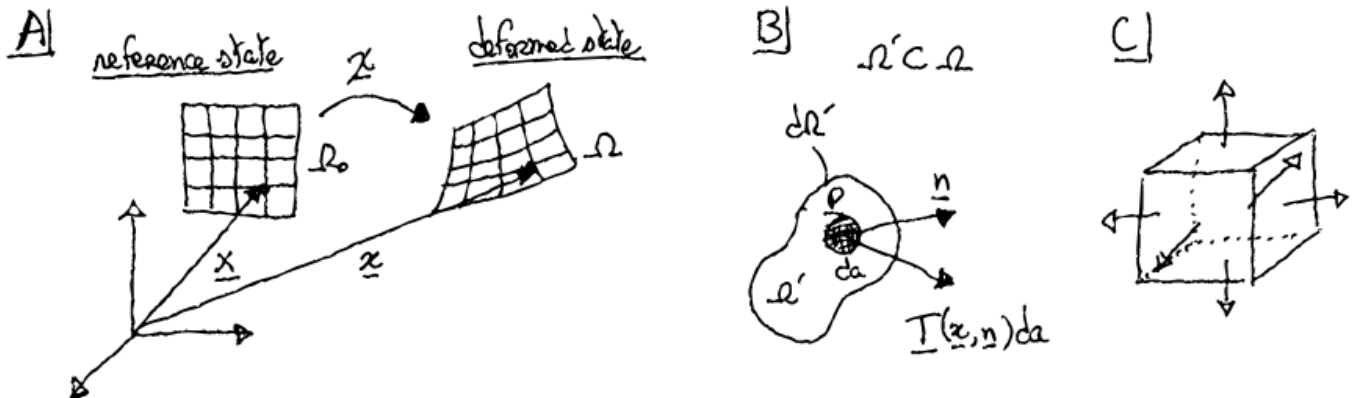


Figure 3.1: (A) Schematics of the mapping χ between the reference and deformed states of the material. (B) Traction force $\underline{T}(s, \underline{n})d\underline{a}$ exerted along the normal \underline{n} at a point P of a subset $\Omega' \subset \Omega$ of the material. (C) Elementary cubic subset of the material with traction forces depicted at each interface.

Deformation

The continuous material occupies a space Ω_0 in the reference state and Ω in the current or deformed state, as represented on Fig. 3.1. Each material point in the reference state is parametrized by a vector \underline{X} and correspondingly by a vector \underline{x} in the deformed state. The material deformation is described by a (invertible) mapping χ , which unambiguously relates \underline{x} and \underline{X} at time t

$$\Omega_0, [0, +\infty[\xrightarrow{\chi} \Omega \quad (3.1)$$

$$\underline{X}, t \mapsto \underline{x} = \chi(\underline{X}, t) \quad (3.2)$$

The velocity of a material (or Lagrangian) point can be defined as

$$\underline{\boldsymbol{v}} = \frac{d\boldsymbol{x}}{dt} = \left. \frac{\partial \boldsymbol{\chi}(\boldsymbol{X}, t)}{\partial t} \right|_{\boldsymbol{X}} \quad (3.3)$$

Deformations may be defined as $\boldsymbol{u}(\boldsymbol{X}) \equiv \boldsymbol{x} - \boldsymbol{X}$, but it is usually useful to define a deformation gradient tensor

$$\underline{\underline{\boldsymbol{F}}} = \frac{\partial \boldsymbol{x}}{\partial \boldsymbol{X}} = \frac{\partial \boldsymbol{\chi}}{\partial \boldsymbol{X}} \quad (3.4)$$

or in cartesian coordinates $F_{ij} = \frac{\partial x_i}{\partial X_j}$. The deformation gradient tensor describes the transport of a material point \boldsymbol{V} in the reference state: $\boldsymbol{v} = \underline{\underline{\boldsymbol{F}}} \cdot \boldsymbol{V}$.

From the deformation tensor we can measure the change in a scalar product between two material vectors defined as \boldsymbol{V} and \boldsymbol{W} (so dilatations) in the reference state by

$$\boldsymbol{v}(t) \cdot \boldsymbol{w}(t) = \boldsymbol{V} \cdot \underline{\underline{\boldsymbol{C}}} \cdot \boldsymbol{W} \quad (3.5)$$

where $\underline{\underline{\boldsymbol{C}}} = \underline{\underline{\boldsymbol{F}}}^T \cdot \underline{\underline{\boldsymbol{F}}}$ is called the dilatation tensor.

Finally, the important measures that one may wish to relate to stress are strains, which measure the variation of scalar products between the reference and current configurations. The strain is quantified in general using the *Green Lagrange strain tensor*

$$\underline{\underline{\boldsymbol{\epsilon}}} \equiv \frac{1}{2} (\underline{\underline{\boldsymbol{C}}} - \underline{\underline{1}}) = \frac{1}{2} (\underline{\underline{\boldsymbol{F}}}^T \cdot \underline{\underline{\boldsymbol{F}}} - \underline{\underline{1}}) \quad (3.6)$$

The material movement is rigid if and only if this tensor vanishes at any point of Ω_0 .

Traction and stress

We consider a subdomain $\Omega' \subset \Omega$ of the material at the current state as represented on Fig. 3.1. The elementary force exerted on the point P at \boldsymbol{x} of the boundary $\partial\Omega'$ of the subdomain reads

$$d\boldsymbol{f} = \boldsymbol{T}(\boldsymbol{x}, \boldsymbol{n}(\boldsymbol{x}))da \quad (3.7)$$

where \boldsymbol{T} is called the traction and is a density of contact forces, $\boldsymbol{n}(\boldsymbol{x}, t)$ is the normal of the boundary at \boldsymbol{x} and da is the elementary area around the point P .

The Cauchy theorem states that the traction at an interface $\boldsymbol{T}(\boldsymbol{x}, \boldsymbol{n}(\boldsymbol{x}))$ is a linear form of the normal of this interface \boldsymbol{n} ¹. This defines the **Cauchy stress tensor**

$$\boldsymbol{T}(\boldsymbol{x}, \boldsymbol{n}(\boldsymbol{x})) = \underline{\underline{\boldsymbol{\sigma}}}(\boldsymbol{x}, t) \cdot \boldsymbol{n}(\boldsymbol{x}, t) \quad (3.8)$$

In cartesian coordinates, this reads $T_i = \sigma_{ij}n_j$ and leads to the elementary traction force expression

$$df_i = \sigma_{ij}n_j da$$

If now we consider an elementary cubic material domain as shown on Fig. 3.1, we can write down the traction force on each interface and takes the limit of infinitely small domain. This leads to the equation for the mechanical equilibrium of the cube²

$$\nabla \cdot \underline{\underline{\boldsymbol{\sigma}}} = \mathbf{0}$$

or in cartesian coordinates $\partial_i \sigma_{ij} = 0$

¹The Cauchy theorem can be demonstrated by writing momentum balance on an elementary tetrahedron and taking the limit of infinitely small volume.

²Here we don't consider external bulk forces on the domain nor acceleration.

Finally, by writing similarly torque balance (conservation of angular momentum) on the elementary cube in the same limit, one can easily prove that the Cauchy stress tensor shall be symmetric

$$\underline{\underline{\sigma}}^t = \underline{\underline{\sigma}} \iff \sigma_{ij} = \sigma_{ji}$$

Conservation equations

There are generally two major conservation equations associated to continuum descriptions: mass conservation and momentum conservation.

Mass conservation reads in all generality

$$\frac{\partial \rho}{\partial t} + \nabla \cdot (\rho \mathbf{v}) = s, \quad (3.9)$$

where ρ is the mass density (or mass per unit area in 2D), \mathbf{v} is the material velocity and s represents material source or sink terms, which in the context of tissue growth and homeostasis, will be linked later to cell growth and apoptosis.

The conservation of momentum reads generally

$$\rho \mathbf{a}(\mathbf{x}, t) = \nabla \cdot \boldsymbol{\sigma}(\mathbf{x}, t) + \mathbf{f}(\mathbf{x}, t).$$

and relates the acceleration $\mathbf{a} = \frac{\partial \mathbf{v}}{\partial t} + (\mathbf{v} \cdot \nabla) \mathbf{v}$ to the Cauchy stress tensor $\boldsymbol{\sigma}$ and external forces \mathbf{f} . In tissues, the inertial term is most generally negligible (overdamped equation), when compared to the divergence of stress, and in the following it will be dropped³, leading to

$$\nabla \cdot \boldsymbol{\sigma}(\mathbf{x}, t) + \mathbf{f}(\mathbf{x}, t) = \mathbf{0}. \quad (3.10)$$

Note that in comparison to the mechanical equilibrium derived in the previous paragraph,, we have considered here possible bulk forces $\mathbf{f}(\mathbf{x}, t)$ on the domain.

3.2 Tissues as active fluids

3.2.1 Active gel theory

In this section we will present a systematic method to derive hydrodynamic equations for a system weakly out-of-equilibrium, relying on Onsager relations [29]. This approach is the one that was used to derive active polar (and nematic) gel theories [30], which generalize hydrodynamic equations for polar (or nematic) liquid crystals to active materials.

Hydrodynamic variables and conservation laws

Hydrodynamic descriptions suppose that there exist variables (called *hydrodynamic* variables), which are degrees of freedom varying 'slowly' in space and time for the system [31]. They are generally of three types: conserved variables, soft modes (associated to broken continuous symmetries of the system) and critical variables. In this specific context, we don't consider systems close to critical points, and we will only work with conserved variables and variables associated to soft modes. The only originality of the approach below is that it applies to an open system, sustained in an out-of-equilibrium state by constant input of (bio)chemical energy. We will suppose that the deviation from equilibrium remains weak in the following.

³The validity of this approximation may be checked in specific examples by relevant dimensionless numbers, such as the *Reynolds number* $\mathcal{R} = \frac{\rho v L}{\eta}$ for a purely viscous material of viscosity η , or the *Mach number* $\mathcal{M} = \frac{v}{\sqrt{E/\rho}} = \frac{v}{c}$ for a purely elastic material (with E the Young modulus, and $c = \sqrt{E/\rho}$ the speed of sound in the material).

Below we describe the tissue as a single phase, made of a single constituent that are the cells themselves. More complex descriptions may account for the extracellular matrix that lies between cells in certain tissues, and couple this additional constituent considering its own rheological model as well [32].

One first obvious candidate for conserved variables is the number density $\rho = \frac{n}{V}$ (with n the number of cells in a tissue), that is associated to the conservation equation⁴:

$$\frac{\partial \rho}{\partial t} + \nabla \cdot \mathbf{j} = \mathbf{0}. \quad (3.11)$$

Defining the velocity $\mathbf{v} = \frac{d\mathbf{x}}{dt}$ of the tissue, which characterizes the flow that transport cells, the current in our context for the density is simply the convective term $\mathbf{j} = \rho\mathbf{v}$.

Another conserved variable is the impulsion $\mathbf{g} = \rho m \mathbf{v}$ (where m is the effective mass of cells), for which one can write a similar conservation equation in the form

$$\frac{\partial \mathbf{g}}{\partial t} + \nabla \cdot \underline{\underline{\Pi}} = \mathbf{0} \quad (3.12)$$

where the momentum flux in the system is $\underline{\underline{\Pi}} = -\underline{\underline{\sigma}}^t + \rho m \mathbf{v} \times \mathbf{v}$. $\underline{\underline{\sigma}}^t$ is the total stress in the system and the second term is called the Reynolds tensor⁵ and accounts for the inertial transport of the impulsion by the velocity⁶.

The last hydrodynamic variable we will consider is associated with a broken continuous symmetry and describes the polarity of cells. We consider indeed that cells may have a preferred orientation, either linked with their shape, or with an intrinsic polarity (biochemical for instance). For instance, in epithelia cells can spontaneously polarize in the apical plane, through interactions between polarity proteins across cellular interfaces. This is called planar-polarity and leads generally to a tendency of neighbouring cells to align with each others, giving rise to large-scale polarity patterns. We therefore introduce a polarization vector $\mathbf{p}(\mathbf{x}, t)$ as hydrodynamic variable to describe cell polarity.

To summarize, we have identified three hydrodynamic variables to describe the state of the tissue: the density $\rho(\mathbf{x}, t)$, the velocity $\mathbf{v}(\mathbf{x}, t)$ and the polarization $\mathbf{p}(\mathbf{x}, t)$.

Entropy production and variation of the free energy

To derive generalized hydrodynamic equations coupling the hydrodynamic variables, we need to write the rate of entropy production *à la* de Groot and Mazur[29] and to identify the generalized fluxes and forces.

We consider the tissue maintained at the temperature T , that means that it is in contact to a heat bath of temperature T , with which it can exchange heat Q and work W ⁷. The first principle of thermodynamics reads

$$\dot{U} = \dot{Q} + \dot{W} \quad (3.13)$$

where the superimposed dot stands denotes the time derivative.

The entropy balance may be written

$$\dot{S} = \frac{\dot{Q}}{T} + \dot{S}_{\text{irr}} \quad (3.14)$$

⁴Note that if sink and source terms are added on the right side of equation (3.11) (to model proliferation and apoptosis for instance), ρ will not be conserved anymore in a strict sense, and to be rigorous the derivation below would need to be changed to account explicitly for the thermodynamics of the exchange with a reservoir of cells. In practice this is however rarely done.

⁵This term appears frequently in turbulence and may be found by averaging the Navier-Stokes equation with a fluctuating velocity [33].

⁶For most active gels, it can be neglected as well as the time derivative of the impulsion (acceleration) because the deformation of tissues is inertialess. This leads to the momentum conservation equation $\nabla \cdot \underline{\underline{\sigma}}^t = \mathbf{0}$. In fact, since mass does not play any role in the following, we will use $\mathbf{v}(\mathbf{x}, t)$ as second independent hydrodynamic variable instead of the impulsion.

⁷In all generality we would have to consider that the system is open as cells gets their nutrients - and therefore their energy - from the bath and we would add a contribution U_e of exchanged energy with a bath. In a similar manner if the number of cells is not constant, an additional energy is required.

where $S(t)$ is the entropy of the tissue, \dot{S}_{irr} is the irreversible entropy production rate of the system. The second principle states that the irreversible entropy production rate is positive $\dot{S}_{\text{irr}} \geq 0$.

Introducing the Helmholtz free energy $F = U - TS$ for the tissue, we can combine the two principles above and we can express the dissipation from the entropy production rate⁸

$$\mathcal{D} \equiv T\dot{S}_{\text{irr}} = \dot{W} - \dot{F} \geq 0. \quad (3.15)$$

The constitutive equations of the system have to satisfy this fundamental inequality.

For a passive gel at rest, the free energy density f of the system is a function of the two intensive variables, the density ρ and the polarization \mathbf{p} and its differential is $df = \mu d\rho - \mathbf{h} \cdot d\mathbf{p}$. The field conjugate to the density is the chemical potential μ , and the field conjugate to the polarization is the orientational field \mathbf{h} [34]. For a passive system moving at a velocity \mathbf{v} , the density of kinetic energy $\frac{1}{2}\mathbf{g} \cdot \mathbf{v} = \frac{1}{2}\rho m\mathbf{v}^2$ must furthermore be added to the free energy.

For an active gel, one must also take into account the fact that energy is constantly injected into the gel locally. A simple and intuitive way to introduce the energy injection is to assume that it is due to a non-equilibrium chemical reaction such as the consumption of ATP (Adenosine TriPhosphate), the unit of energy in a cell. We denote $\Delta\mu$ the chemical potential associated to the hydrolysis of one ATP molecule into ADP (adenosine diphosphate) and an inorganic phosphate. It corresponds to the energy gain per ATP molecule of the hydrolysis of the reaction, whose rate of advancement (number of ATP consumed per unit time and unit volume) is noted r . The associate rate of change of the free energy per unit volume is calculated as $-r\Delta\mu$. Taking all contributions, the time variation of the free energy reads

$$\frac{dF}{dt} = \int_V d\mathbf{r} \left\{ \mu \frac{\partial \rho}{\partial t} - \mathbf{h} \cdot \frac{\partial \mathbf{p}}{\partial t} + \frac{\partial}{\partial t} \left(\frac{1}{2}\mathbf{g} \cdot \mathbf{v} \right) - r\Delta\mu \right\} \quad (3.16)$$

To make explicit the expression of orientational field $\mathbf{h} = -\frac{\delta F_p}{\delta \mathbf{p}}$, we need to define a polarization free energy F_p . The polarization energy in 3 dimensions is a functional of the three components of the polarization vector \mathbf{p} . However, if the system is not in the vicinity of a critical point, there are only two soft modes associated with rotations of the polarization: the modulus of the polarization is not a hydrodynamic variable and is taken to be constant. Without loss of generality, we can consider it as a unit vector. One common choice for a polarization free energy is to take the Frank energy of a nematic liquid crystal[34]:

$$F_p = \int_V d\mathbf{r} \left\{ \frac{K_1}{2} (\nabla \cdot \mathbf{p})^2 + \frac{K_2}{2} (\mathbf{p} \cdot (\nabla \times \mathbf{p}))^2 + \frac{K_3}{2} (\mathbf{p} \times (\nabla \times \mathbf{p}))^2 - \frac{1}{2} h_{\parallel}^0 (\mathbf{p}^2 - 1) \right\} \quad (3.17)$$

This energy was obtained by Frank using symmetry arguments and developing the energy up to the second order in $\nabla \mathbf{p}$ ⁹. The three first terms correspond to the energies associated to splay, twist and bend deformations (see Fig. 3.2), where the Frank constants K_i are considered positive. h_{\parallel}^0 is a Lagrange multiplier to ensure that \mathbf{p} is a unit vector¹⁰. In general it is useful to decompose the orientational field as $\mathbf{h} = -\frac{\delta F_p}{\delta \mathbf{p}} = h_{\parallel} \mathbf{p} + \mathbf{h}_{\perp}$, where the first term $h_{\parallel} = \mathbf{h} \cdot \mathbf{p}$ is parallel to the polarization and the second term $\mathbf{h}_{\perp} = (\mathbf{h} - (h_{\parallel} \mathbf{p}))$ is perpendicular to the polarization. \mathbf{h}_{\perp} may be seen as a driving force density, which tends to minimize gradients of polarization.

⁸Considering explicitly exchanges, one would have to consider an additional positive free energy term $F_e = U_e - TS_e$ in the dissipation.

⁹Here we did not consider terms linear in \mathbf{p} , because we suppose the system essentially nematic, that is following the symmetry $\mathbf{p} \rightarrow -\mathbf{p}$. For a polar system an additional term $k\nabla \cdot \mathbf{p}$ shall be added to the Frank energy, and leads to a surface contribution only if $k = \text{cte}$ by the Green-Ostrogradski theorem.

¹⁰This constraint of unit vector is an approximation, and means that we neglect fluctuations in our mesoscopic volume, by supposing that the polarization of each cell in this volume is exactly \mathbf{p} .

In the next we consider the simplifying case where all Frank constants are equal $K_1 = K_2 = K_3 = K$, which simplifies the energy into

$$F_p = \frac{1}{2} \int_V d\mathbf{r} \left\{ K \|\nabla \mathbf{p}\|^2 - h_{\parallel}^0 (\mathbf{p}^2 - 1) \right\} = \frac{1}{2} \int_V d\mathbf{r} \left\{ K \left[(\nabla \cdot \mathbf{p})^2 + |\nabla \times \mathbf{n}|^2 \right] - h_{\parallel}^0 (\mathbf{p}^2 - 1) \right\} \quad (3.18)$$

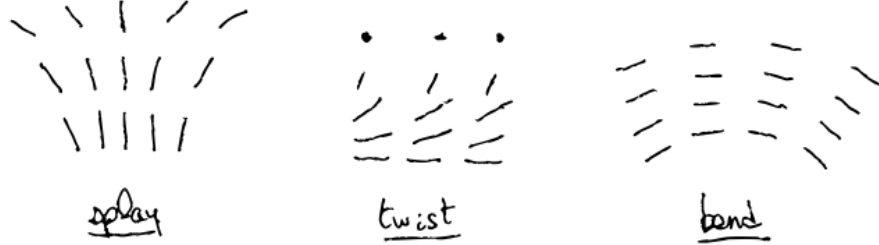


Figure 3.2: Deformations in nematics: splay, bend and twist.

In the simple case of a 2-dimensional system, the polarization is simply characterized by its polar angle θ ($\mathbf{p} \cdot \mathbf{e}_x = \cos \theta$) and the Frank energy reads then

$$F_p^{2D} = \frac{1}{2} K \int_A d\mathbf{r} (\nabla \theta)^2 =$$

. The perpendicular part of the orientational field becomes then simply $h_{\perp} = K \nabla^2 \theta$, which means that the equilibrium with respect to polarization is obtained for $\nabla^2 \theta = 0$.

In a non-isotropic medium, such as nematic tissues, the total stress is not symmetric anymore. There is an antisymmetric component of the stress associated to torques in the medium. This anti-symmetric component can be calculated from the conservation of momentum and is equal to¹¹

$$\sigma^A = \frac{1}{2} (h_{\alpha} p_{\beta} - p_{\alpha} h_{\beta})$$

Considering a pressure P to ensure the incompressibility constraint in the gel, the total stress $\underline{\sigma}^t$ may be decomposed as follows

$$\sigma_{\alpha\beta}^t = \sigma_{\alpha\beta} + \sigma_{\alpha\beta}^A - P \delta_{\alpha\beta} \quad (3.19)$$

The component $\sigma_{\alpha\beta}$ is symmetric and is called the deviatoric stress tensor.

Fluxes, forces and time-reversal

According to Onsager theory entropy production (or dissipation) is the sum of terms that are products of generalized hydrodynamic fluxes and hydrodynamic forces. Close to thermodynamic equilibrium, the generalized fluxes entering in the dissipation can be written as a linear combination (with some symmetries on the kinetic coefficients) of the generalized forces[29]. Below, we will therefore start from (minus) the rate of change of the free energy to deduce the entropy production.

¹¹If the system is chiral, the antisymmetric part of the stress takes a different form, and needs to be calculated in details, see [35].

We use conservation laws and perform an integration by parts of minus the time derivative of the free energy:

$$\begin{aligned}
-\frac{dF}{dt} &= - \int_V d\mathbf{r} \left\{ \mu \frac{\partial \rho}{\partial t} - \mathbf{h} \cdot \frac{\partial \mathbf{p}}{\partial t} + \frac{\partial}{\partial t} \left(\frac{1}{2} \rho m \mathbf{v}^2 \right) - r \Delta \mu \right\} \\
&= \int d\mathbf{r} \left\{ \mu \nabla \cdot (\rho \mathbf{v}) + \mathbf{h} \cdot \frac{\partial \mathbf{p}}{\partial t} + (\nabla \cdot \underline{\Pi}) \cdot \mathbf{v} + r \Delta \mu \right\} \\
&\quad \text{where we used the two conservation laws for } \mathbf{g} \text{ and } \rho \\
&= \int d\mathbf{r} \left\{ \mu \partial_\alpha (\rho v_\alpha) + h_\alpha \frac{\partial p_\alpha}{\partial t} - \partial_\alpha \sigma_{\alpha\beta}^t v_\beta + r \Delta \mu \right\} \\
&\quad \text{where we used the definition } \Pi_{\alpha\beta} = -\sigma_{\alpha\beta}^t + \rho m v_\alpha v_\beta \text{ and dropped inertial terms.} \\
&= \int d\mathbf{r} \left\{ -\rho v_\alpha \partial_\alpha \mu + h_\alpha \frac{\partial p_\alpha}{\partial t} + \sigma_{\alpha\beta}^t \partial_\alpha v_\beta + r \Delta \mu \right\} \\
&\quad \text{where we performed integrations by parts.}
\end{aligned}$$

At this point, we need an additional relation between the density and the pressure in the fluid. This is the Gibbs-Duhem relation, which for a nematic fluid [34] reads¹²

$$dP - \frac{S}{V} dT = \rho d\mu + \mathbf{h} \cdot d\mathbf{p} \quad (3.20)$$

where $dT = 0$ because the tissue is in contact with a thermal bath. Replacing in minus the rate of change of the free energy above leads to

$$\begin{aligned}
-\frac{dF}{dt} &= \int d\mathbf{r} \left\{ -v_\alpha (\partial_\alpha P - h_\beta \partial_\alpha p_\beta) + h_\alpha \frac{\partial p_\alpha}{\partial t} + \sigma_{\alpha\beta}^t \partial_\alpha v_\beta + r \Delta \mu \right\} \\
&= \int d\mathbf{r} \left\{ P \delta_{\alpha\beta} \partial_\alpha v_\beta + h_\beta v_\alpha \partial_\alpha p_\beta + h_\alpha \frac{\partial p_\alpha}{\partial t} + \sigma_{\alpha\beta} \partial_\alpha v_\beta + \frac{1}{2} (h_\alpha p_\beta - p_\alpha h_\beta) \partial_\alpha v_\beta - P \delta_{\alpha\beta} \partial_\alpha v_\beta + r \Delta \mu \right\} \\
&\quad \text{where we integrated by part and used the definition of } \sigma_{\alpha\beta}^t \\
&= \int d\mathbf{r} \left\{ \sigma_{\alpha\beta} \partial_\alpha v_\beta + h_\alpha \left(\frac{\partial p_\alpha}{\partial t} + v_\beta \partial_\beta p_\alpha + \frac{1}{2} (p_\beta \partial_\alpha v_\beta - p_\alpha \partial_\beta v_\alpha) \right) + r \Delta \mu \right\} \\
&= \int d\mathbf{r} \{ \sigma_{\alpha\beta} v_{\alpha\beta} + h_\alpha P_\alpha + r \Delta \mu \}
\end{aligned} \quad (3.21)$$

where we introduced the convected corotational time derivative of the polarization

$$P_\alpha \equiv \frac{Dp_\alpha}{Dt} = \frac{\partial p_\alpha}{\partial t} + v_\beta \partial_\beta p_\alpha + \omega_{\alpha\beta} p_\beta \quad (3.22)$$

the vorticity (antisymmetric) tensor

$$\underline{\omega} = \frac{1}{2} \nabla \times \mathbf{v} \leftrightarrow \omega_{\alpha\beta} = \frac{1}{2} (\partial_\alpha v_\beta - \partial_\beta v_\alpha) \quad (3.23)$$

and the (symmetric) strain rate tensor (because $\sigma_{\alpha\beta}$ is symmetric)

$$v_{\alpha\beta} = \frac{1}{2} (\partial_\alpha v_\beta + \partial_\beta v_\alpha) \quad (3.24)$$

¹²The relation of Gibbs-Duhem ensures the extensivity of the variables ρ and \mathbf{h} .

This form of free energy (3.21) may be read by identifying pairs of conjugate generalized fluxes and forces

$$\text{flux} \leftrightarrow \text{force} \quad (3.25)$$

$$\sigma_{\alpha\beta} \leftrightarrow v_{\alpha\beta} \quad (3.26)$$

$$P_\alpha \leftrightarrow h_\alpha \quad (3.27)$$

$$r \leftrightarrow \Delta\mu \quad (3.28)$$

$$(3.29)$$

The rate of change of the free energy (3.21) can be divided into an irreversible part $\dot{F} = \dot{F}_{\text{rev}} + \dot{F}_{\text{irr}} = \dot{W} - T\dot{\mathcal{S}}$ (see (3.15)). We therefore decompose the fluxes into reactive and dissipative parts as well. They are characterized by their different signature with respect to time-reversal, and will depend on the - well-defined - signature of generalized forces under time-reversal: $v_{\alpha\beta}$ has a signature -1 (because the velocity has a signature -1), while h_α and $\Delta\mu$ have a signature $+1$. We write

$$\sigma_{\alpha\beta} = \sigma_{\alpha\beta}^r + \sigma_{\alpha\beta}^d \quad (3.30)$$

$$P_\alpha = P_\alpha^r + P_\alpha^d \quad (3.31)$$

$$r = r^r + r^d \quad (3.32)$$

To satisfy the second principle of thermodynamics $T\dot{\mathcal{S}} \geq 0$, the dissipative fluxes have the same signature under time reversal as their conjugate forces, while reactive fluxes have the opposite signature. Therefore, $\sigma_{\alpha\beta}^d$ has a signature -1 , and r^d and P_α^d have a signature $+1$. Reactive parts have correspondingly opposite signatures.

The rate of entropy production $T\dot{\mathcal{S}} = -\dot{F}_{\text{irr}}$ reads therefore

$$T\dot{\mathcal{S}} = \int d\mathbf{r} \left\{ \sigma_{\alpha\beta} v_{\alpha\beta}^d + h_\alpha P_\alpha^d + r^d \Delta\mu \right\} \quad (3.33)$$

Now we can write down the Onsager relations, that is all the possible linear relations between forces and fluxes, as far as they respect the symmetry of the system and have either the same time-reversal signature for dissipative fluxes or opposite time-reversal signature for reactive fluxes. Respecting symmetries of the system means that vectors can be constructed only with vectors and gradients, but gradients are supposed subdominant (slowly varying hydrodynamic variables), and tensors can be constructed with $\delta_{\alpha\beta}$ or $q_{\alpha\beta} = p_\alpha p_\beta - \frac{1}{3}\delta_{\alpha\beta}$.

By convenience, we split all tensors into diagonal and traceless parts: $\sigma_{\alpha\beta} = \sigma\delta_{\alpha\beta} + \tilde{\sigma}_{\alpha\beta}$, with $\sigma = \frac{1}{3}\sigma_{\alpha\alpha}$ and $\tilde{\sigma}_{\alpha\alpha} = 0$. Similarly, we write $v_{\alpha\beta} = \bar{v}\delta_{\alpha\beta} + \tilde{v}_{\alpha\beta} = \bar{v}\delta_{\alpha\beta}$.

Dissipative fluxes. Only fluxes and forces with the same time-reversal signature are coupled. For the stress tensor, this leads to

$$\sigma^d = \bar{\eta}\frac{\bar{v}}{3} \quad (3.34a)$$

$$\tilde{\sigma}_{\alpha\beta}^d = 2\eta\tilde{v}_{\alpha\beta} \quad (3.34b)$$

where $\bar{\eta}$ is the longitudinal viscosity while η is called the shear viscosity¹³

The two other fluxes are coupled and the corresponding constitutive equations read

$$P_\alpha^d = \frac{h_\alpha}{\gamma} + \lambda p_\alpha \Delta\mu \quad (3.35)$$

¹³In all generality, the most generic linear combination between the stress and strain tensors is described by a viscosity tensor or rank 4 $\tilde{\sigma}_{\alpha\beta}^d = \eta^{\gamma\delta}_{\alpha\beta}\tilde{v}_{\gamma\delta}$

and

$$r^d = \Lambda\Delta\mu + \lambda p_\alpha h_\alpha \quad (3.36)$$

because h_α and $\Delta\mu$ have the same signature +1. Note that the coefficient λ is the same because the matrix of coefficients shall be symmetric (Onsager relations).

Reactive fluxes. The reactive Onsager matrix is antisymmetric and couples fluxes and forces of opposite time reversal signatures:

$$\sigma^r = -\bar{\zeta}\Delta\mu + \bar{\nu}p_\alpha h_\alpha \quad (3.37a)$$

$$\tilde{\sigma}_{\alpha\beta}^r = -\zeta\Delta\mu q_{\alpha\beta} + \frac{\nu}{2} \left(p_\alpha h_\beta + p_\beta h_\alpha - \frac{2}{3}p_\gamma h_\gamma \delta_{\alpha\beta} \right) \quad (3.37b)$$

$$P_\alpha^r = -\bar{\nu}p_\alpha \frac{\bar{v}}{3} - \nu_1 p_\beta \tilde{v}_{\alpha\beta} \quad (3.37c)$$

$$r^r = \bar{\zeta} \frac{\bar{v}}{3} + \zeta q_{\alpha\beta} \tilde{v}_{\alpha\beta} \quad (3.37d)$$

In the following, we will consider an incompressible tissue, such that $\bar{v} = \nabla \cdot \mathbf{v} = 0$. In this case, the diagonal component of the stress can be included in the pressure, which is a Lagrange multiplier ensuring incompressibility and one can set $\bar{\zeta} = \bar{\nu} = \bar{\eta} = 0$

Summary of the active tissue model

In summary, the hydrodynamic equations for an incompressible one-component active tissue of nematic symmetry are given by

$$m\rho(\partial_t + \mathbf{v} \cdot \nabla)\mathbf{v} = -\nabla P + \nabla \cdot \underline{\underline{\sigma}}^t \quad (3.38a)$$

$$(\partial_t + v_\beta \partial_\beta)p_\alpha + \omega_{\alpha\beta}p_\beta = -\nu v_{\alpha\beta}p_\beta + \frac{1}{\gamma}h_\alpha + \lambda\Delta\mu p_\alpha \quad (3.38b)$$

to be supplemented with the incompressibility condition $\nabla \cdot \mathbf{v} = 0$, the expression of the molecular field (for the approximation of one Frank constant)

$$h_\alpha = K\nabla^2 p_\alpha + h_\parallel^0 p_\alpha \quad (3.39)$$

where h_\parallel^0 is a Lagrange multiplier to be determined from the constraint $|\mathbf{p}| = 1$. Finally the total stress tensor is the sum of deviatoric and trace parts of the dissipative and reactive components plus the anti-symmetric component, and may be conveniently separated into passive and active parts $\sigma_{\alpha\beta}^t = \sigma_{\alpha\beta}^p + \sigma_{\alpha\beta}^a$ where

$$\sigma_{\alpha\beta}^p = 2\eta\tilde{v}_{\alpha\beta} + \frac{\nu}{2} \left(p_\alpha h_\beta + p_\beta h_\alpha - \frac{2}{3}p_\gamma h_\gamma \delta_{\alpha\beta} \right) - \frac{1}{2}(p_\alpha h_\beta - h_\alpha p_\beta), \quad (3.40a)$$

$$\sigma_{\alpha\beta}^a = -\zeta\Delta\mu q_{\alpha\beta} \quad (3.40b)$$

3.2.2 Application: spontaneous flow in a confined epithelium

Here we present an instability which has been observed in tissues cultured *in vitro* in a confined situation [36].

As sketched on Fig. 3.3, we consider a 2-dimensional epithelium confined between two flat boundaries separated by a distance L along the direction x . The tissue is supposed long enough in the y -direction to suppose invariance by translation along y . To quantify the elongation of cells, we introduce $r(\theta)$ the position

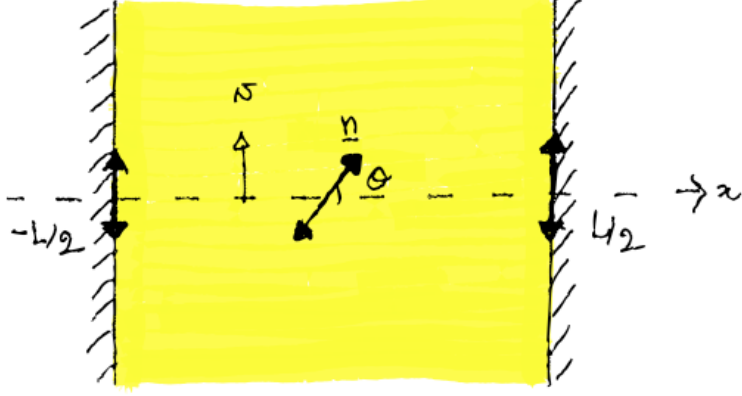


Figure 3.3: Sketch of the 2-dimensional tissue in confinement between two plates, separated by a length L and supposed invariant along y . \mathbf{n} is the director field and the velocity field is denoted by \mathbf{v}

of the contour of a cell in polar coordinates away from the cell center, with θ the angle made with the basis vector \mathbf{e}_x . One could, in principle, introduce a polarization vector of cells

$$\mathbf{p}^{\text{cell}} = \frac{1}{2\pi R} \begin{pmatrix} \int_0^{2\pi} d\theta r(\theta) \cos \theta \\ \int_0^{2\pi} d\theta r(\theta) \sin \theta \end{pmatrix} \quad (3.41)$$

where we introduced $R = \frac{1}{2\pi} \int_0^{2\pi} d\theta r(\theta)$ the average radius of cells. Nevertheless, the shape of cells is better characterized by a nematic order parameter, which does not include a notion of polarity

$$\underline{\underline{Q}}^{\text{cell}} = \frac{1}{2\pi R} \begin{pmatrix} \int_0^{2\pi} d\theta r(\theta) \cos(2\theta) & \int_0^{2\pi} d\theta r(\theta) \sin(2\theta) \\ \int_0^{2\pi} d\theta r(\theta) \sin(2\theta) & -\int_0^{2\pi} d\theta r(\theta) \cos(2\theta) \end{pmatrix} \quad (3.42)$$

which is a symmetric and traceless tensor. We can rewrite this tensor as follows

$$\underline{\underline{Q}}^{\text{cell}} = 2S \begin{pmatrix} n_x^2 - \frac{1}{2} & n_x n_y \\ n_x n_y & n_y^2 - \frac{1}{2} \end{pmatrix} \quad (3.43)$$

with $S \equiv \sqrt{(Q_{xx}^{\text{cell}})^2 + (Q_{yy}^{\text{cell}})^2}$ and we introduced a normalized nematic director \mathbf{n} such that $\mathbf{n}^2 = 1$. Both \mathbf{n} and $-\mathbf{n}$ lead to the same tensor $\underline{\underline{Q}}^{\text{cell}}$, as required by the fact that the nematic order parameter shall not vary by a rotation of π .

In the next, we will consider a mean local cell elongation tensor, averaged over a certain mesoscopic area containing a sufficient number of cells α

$$\underline{\underline{Q}} = \left\langle \underline{\underline{Q}}^{\text{cell}} \right\rangle = \frac{\sum_\alpha A_\alpha \underline{\underline{Q}}_\alpha}{\sum_\alpha A_\alpha} \quad (3.44)$$

This definition gives less weight to cells that occupy a smaller area in the 2-dimensional tissue.

The director $\mathbf{n} = (\cos \theta, \sin \theta)$ allows us to precise the boundary conditions of the cell elongation in this system $\theta(-\frac{L}{2}) = \theta(\frac{L}{2}) = \frac{\pi}{2}$. Furthermore, the tissue is free to slide along boundaries, such that $\sigma_{xy}(-\frac{L}{2}) = \sigma_{xy}(\frac{L}{2}) = 0$

We assume that the tissue is described by active viscous nematic hydrodynamic equations, as derived in the previous subsection:

$$\sigma_{ij}^t = -P\delta_{ij} + 2\eta\tilde{v}_{ij} + \zeta\Delta\mu \left[n_i n_j - \frac{1}{2}\delta_{ij} \right] + \frac{\nu}{2} \left(n_i h_j + n_j h_i - \frac{1}{2}n_k h_k \delta_{ij} \right) - \frac{1}{2}(n_i h_j - n_j h_i) \quad (3.45)$$

$$\partial_t n_i + v_j \partial_j n_i + \omega_{ij} n_j = \frac{1}{\gamma} h_i - \nu \tilde{v}_{ij} n_j \quad (3.46)$$

where we have included the pressure into the total stress. In absence of inertia, momentum conservation is given here simply by

$$\partial_i \sigma_{ij}^t = 0$$

We further assume the tissue incompressible $\partial_i v_j = 0$, and the pressure P is the Lagrange multiplier enforcing this constraint. The molecular field derives from the Frank energy

$$\mathcal{F}_F = \int_S d^2 \mathbf{r} \left[\frac{K}{2} (\nabla \mathbf{n})^2 + \frac{\lambda}{2} (\mathbf{n}^2 - 1) \right] \quad (3.47)$$

where λ is the Lagrange multiplier enforcing $\mathbf{n}^2 = 1$, and reads

$$h_i = -\frac{\partial \mathcal{F}}{\partial n_i} = K \Delta n_i - \lambda n_i \quad (3.48)$$

In 2 dimensions, it can be rewritten

$$h_x = -[K(\partial_x \theta)^2 + \lambda] \cos \theta - K(\partial_x^2 \theta) \sin \theta \quad (3.49a)$$

$$h_y = -[K(\partial_x \theta)^2 + \lambda] \sin \theta + K(\partial_x^2 \theta) \cos \theta \quad (3.49b)$$

We introduce $h_{\parallel} = n_x h_x + n_y h_y$ and $h_{\perp} = n_y h_x - n_x h_y$, the components of \mathbf{h} parallel and perpendicular to \mathbf{n} :

$$h_{\parallel} = -[K(\partial_x \theta)^2 + \lambda] \quad (3.50a)$$

$$h_{\perp} = -K(\partial_x^2 \theta) \quad (3.50b)$$

In absence of flow, at steady-state, the above equations lead to $\mathbf{h} = K \Delta \mathbf{n} - \lambda \mathbf{n} = \mathbf{0}$. To satisfy the boundary conditions, the only possible solution is $\theta = \frac{\pi}{2}$.

The goal now is to study the stability of this solution. In the case where the solution is unstable, a distortion in the cell elongation pattern and a spontaneous flow can emerge in the 2D tissue. To study the stability of the system, we perturb the equilibrium solution $\theta = \frac{\pi}{2} + \delta\theta$, where $\delta\theta \ll 1$.

The incompressibility condition implies $\partial_x v_x + \partial_y v_y = \partial_x v_x = 0$, and v_x shall vanish at the walls, such that $v_x = 0$. The polarity dynamics gives

$$\partial_t n_x + \frac{1}{2} (\partial_x v_y) n_y = \frac{1}{\gamma} h_x - \frac{\nu}{2} (\partial_x v_y) n_y \quad (3.51a)$$

$$\partial_t n_y - \frac{1}{2} (\partial_x v_y) n_x = \frac{1}{\gamma} h_y - \frac{\nu}{2} (\partial_x v_y) n_x \quad (3.51b)$$

where we have used $\omega_{xy} = \frac{1}{2} \partial_x v_y$ and $\omega_{yx} = -\frac{1}{2} \partial_x v_y$. Noting the identity

$$\partial_t \theta = n_x (\partial_t n_y) - n_y (\partial_t n_x)$$

and the (3.50b), we get

$$\partial_t \theta = \frac{K}{\gamma} \partial_x^2 \theta - \frac{\partial_x v_y}{2} (-1 + \nu \cos(2\theta)) \quad (3.52)$$

which, in the limit $\delta\theta \ll 1$, becomes

$$\partial_t \theta = \frac{K}{\gamma} \partial_x^2 \delta\theta + \frac{1+\nu}{2} \partial_x v_y \quad (3.53)$$

To determine the solution for the flow profile v_y , we write the force balance taking into account of the invariance along y :

$$\partial_x \sigma_{xx} = 0, \quad \partial_x \sigma_{xy} = 0.$$

Since $\sigma_{xy} = 0$ at the boundaries, we have uniformly $\sigma_{xy} = 0$ in the tissue, which reads

$$\eta \partial_x v_y + \nu \cos \theta \sin \theta h_{\parallel} + \frac{\nu}{2} (\sin^2 \theta - \cos^2 \theta) h_{\perp} + \frac{1}{2} h_{\perp} + \zeta \Delta \mu \cos \theta \sin \theta = 0 \quad (3.54)$$

where we used the fact that

$$\begin{aligned} n_x h_y + n_y h_x &= \cos \theta (h_{\parallel} \sin \theta - h_{\perp} \cos \theta) + \sin \theta (h_{\parallel} + h_{\perp} \sin \theta) \\ &= 2h_{\parallel} \cos \theta \sin \theta + (\sin^2 \theta - \cos^2 \theta) h_{\perp} \end{aligned} \quad (3.55)$$

Moreover, since $\mathbf{n} = 1$, we have the relation

$$0 = \mathbf{n} \cdot \partial_t \mathbf{n} = n_x (\partial_t n_x) + n_y (\partial_t n_y) = \frac{h_{\parallel}}{\gamma} - \nu (\partial_x v_y) n_x n_y,$$

which yields

$$h_{\parallel} = \nu \gamma (\partial_x v_y) n_x n_y \quad (3.56)$$

Using the expressions for h_{\parallel} and h_{\perp} , (3.54) reads

$$(\eta + \nu^2 \gamma \cos^2 \theta \sin^2 \theta) \partial_x v_y - \frac{K}{2} \partial_x^2 \theta (1 - \nu \cos(2\theta)) + \zeta \Delta \mu \cos \theta \sin \theta = 0 \quad (3.57)$$

which becomes, in the limit $\delta\theta \ll 1$

$$\partial_x v_y = \frac{K}{2\eta} (1 + \nu) \partial_x^2 \delta\theta + \frac{\zeta \Delta \mu}{\eta} \delta\theta \quad (3.58)$$

Combining (3.53) and (3.58), we obtain a differential equation for the orientation of the angular field $\delta\theta$

$$\partial_t \delta\theta = K \left(\frac{1}{\gamma} + \frac{(1 + \nu)^2}{4\eta} \right) \partial_x^2 \delta\theta + \frac{\zeta \Delta \mu (1 + \nu)}{2\eta} \delta\theta \quad (3.59)$$

Using an ansatz $\delta\theta = \epsilon(t) \cos(\frac{\pi x}{L})$ for the solution, we get

$$\partial_t \epsilon = \left[\frac{\zeta \Delta \mu (1 + \nu)}{2\eta} - K \left(\frac{1}{\gamma} + \frac{(1 + \nu)^2}{4\eta} \right) \frac{\pi^2}{L^2} \right] \epsilon \quad (3.60)$$

which exhibits an instability (exponentially growing solution when

$$\frac{\zeta \Delta \mu (1 + \nu)}{2\eta K} > \left(\frac{1}{\gamma} + \frac{(1 + \nu)^2}{4\eta} \right) \frac{\pi^2}{L^2}$$

which defines a critical length L_c above which the tissue becomes unstable

$$L > L_c \equiv \pi \sqrt{\frac{K}{\zeta \Delta \mu}} \sqrt{\frac{2\eta}{\gamma(1 + \nu)}} + \frac{1 + \nu}{2} \quad (3.61)$$

The tissue becomes therefore unstable for a **contractile** tissue $\zeta \Delta \mu > 0$ and for large enough confinement length L . If the length of confinement is too small, distortions in the nematic orientation become energetically too costly and the instability does not develop.

Experimentally, this instability is indeed observed (Fig. 3.4) above a well-defined critical length of length, as shown on Fig. 3.5.

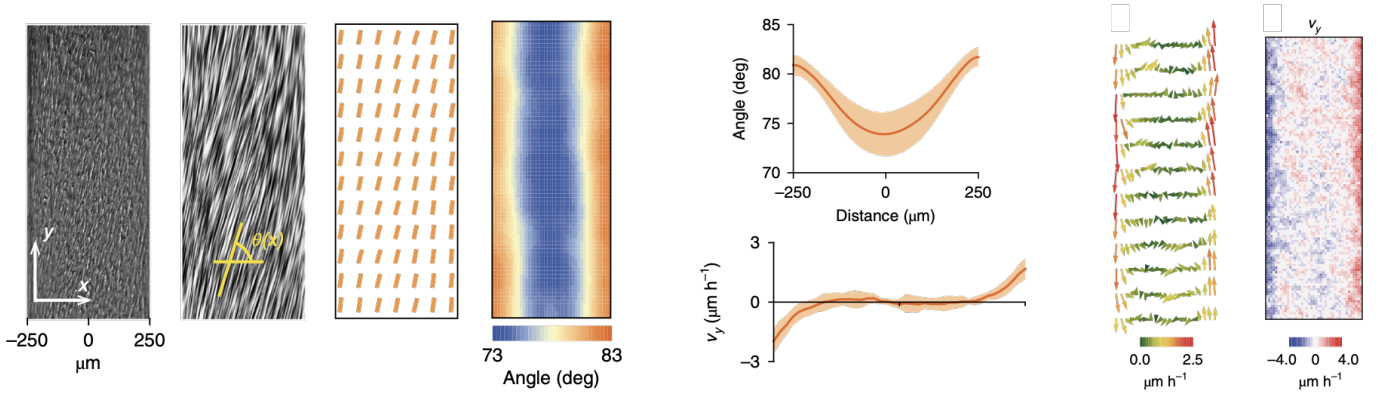


Figure 3.4: Spontaneous flow profile and angle profile in a confined 2-dimensional tissue made of RPE1 cells [36].

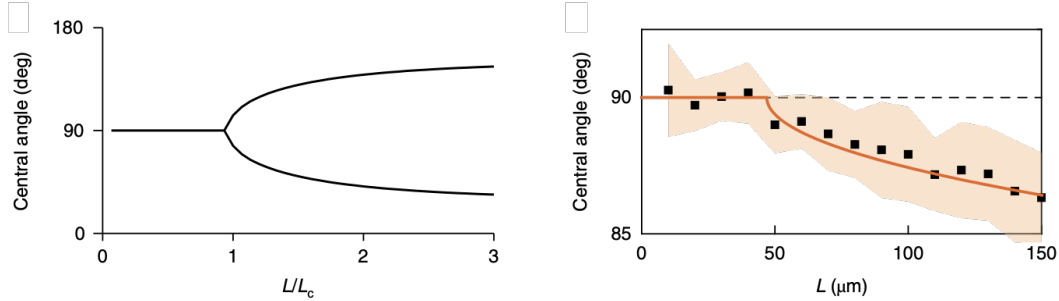


Figure 3.5: Bifurcation diagrams predicted theoretically (left) and found experimentally (right) in [36].

3.2.3 Topological defects

We consider a 2-dimensional nematic tissue, and suppose that the distortion of its director field $\mathbf{n} = (\cos \phi, \sin \phi)$ is controlled by the Frank-Oseen energy $\mathcal{F} = \int_S d^2 r \frac{K}{2} (\partial_i \mathbf{n})^2 = \int_S d^2 r \frac{K}{2} (\partial_i \phi)^2$. The angles ϕ and $\phi + \pi$ refer to the same nematic state. Minimizing this energy with respect to θ , yields a Poisson equation $\Delta \phi = 0$, where $\Delta = \partial_x^2 + \partial_y^2$ is the Laplacian operator.

Cellular elongation patterns of tissues, like for nematic liquid crystals, can exhibit topological defects. A defect is a point where the nematic angle is not defined. These defects can be classified according to their topological charge, which is defined by

$$m = \frac{1}{2\pi} \oint_C d\ell_i \partial_i \phi \quad (3.62)$$

where C is a curve of positive orientation that encloses the charge.

The topological charges quantifies how much the director field rotates along the curve and does not depend on the precise shape of the curve C : a full rotation in the clockwise direction corresponds to a charge $+1$, and in the anticlockwise direction to a charge -1 .

One can find the nematic orientation profile around a defect using the polar expression of the Laplacian operator $\Delta = \partial_r^2 + \frac{1}{r} \partial_r + \frac{1}{r^2} \partial_\theta^2$. A solution that does not depend on r leads to

$$\phi(\theta) = m\theta + \phi_0 \quad (3.63)$$

where m is the nematic charge of the defect.

Since the direction of \mathbf{n} must be well-defined at each point, one has the constraint

$$\oint_\theta d\phi = 2\pi m = k\pi \quad (3.64)$$

where $k \in \mathbb{Z}$. For nematic defect, m must be a multiple of $1/2$ to ensure periodicity and nematic symmetry ($\phi \leftrightarrow \phi + \pi$). The constant angle ϕ_0 corresponds simply to a solid rotation of the defect.

Inserting (3.63) into the Frank energy, the distortion energy associated with a defect of charge m can be calculated as $\mathcal{F}_m = \pi K m^2 \log \frac{R}{r_c}$, where R and r_c are upper and lower cutoff radii around the defect. Hence, a defect with a lower topological charge has a smaller energy and is favored.

On Fig.3.6, we show the corresponding solutions for the lowest-charge defects $m = +1/2$ and $m = -1/2$.

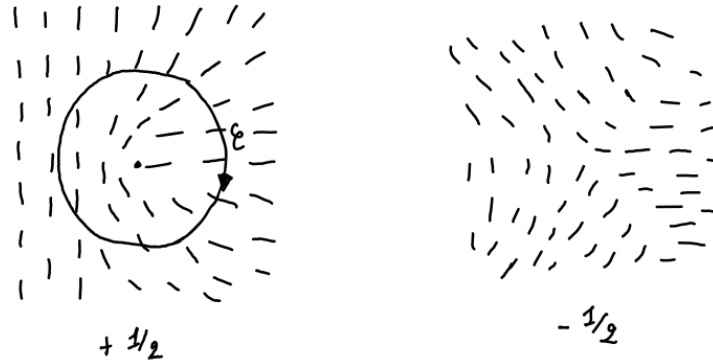


Figure 3.6: Topological defects and nematic orientation profiles for charge defects $m = \frac{1}{2}$ and $m = -\frac{1}{2}$.

One should note that the two $\pm 1/2$ defects have different symmetries: the $+1/2$ defect has a preferred direction (left to right here), while the $-1/2$ has a 3-fold rotational symmetry, and it cannot acquire a velocity.

Experimentally, Duclos et al. [37] have observed patterns of elongated cells cultured *in vitro* (NIH 3T3 mouse embryo fibroblasts) grown on circular discs. The cells tend to orient their axis of elongation parallel to the external interface, as often observed both *in vitro* and *in vivo*. On a disc this enforces a total topological charge of $+1$; therefore defects must arise within the tissue. The number of visible nematic defects decrease over time as the tissue dynamically rearranges and defects of opposite charge annihilate. Eventually the system converges to an organization with only two $+1/2$ defects which form at a reliable distance within the disc. This is consistent with the effective energy argument: the system prefers to choose defect with low charges. In fact, even the final position of defects is also predicted by minimizing the effective distortion energy.

Chapter 4

Continuous models of tissues - tissue growth

This chapter focuses on tissues studied on time-scales longer than the cell cycle (typically several days), where cell divisions and apoptosis need to be taken into account in the mechanical description. Cell division is essential for the morphogenesis of embryonic tissues and organs, which need to grow to adopt their adult size, for the permanent renewal of cells in most tissues, like in the gut, and is also one of the driving force of cancerous tumors, which grow against other tissues.

In the next, we will focus mainly on the last type of tissues, in the form of multicellular spheroids made of immortalized cancerous cell lines, which can be studied *in vitro*.

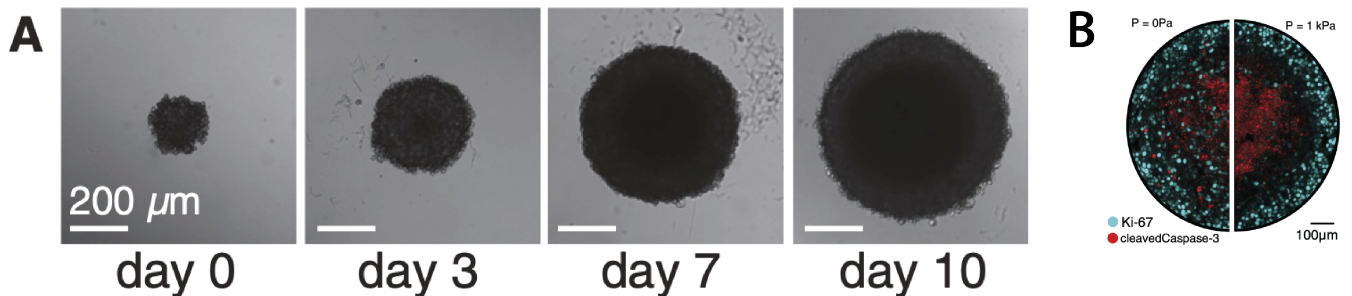


Figure 4.1: Growth of a cellular spheroid. (A) Snapshots of the time evolution of a spheroid made of CT26 mouse carcinoma cells [38]. (B) Distribution of proliferation and apoptosis in a spheroid (cyan corresponds to proliferation, red to apoptosis) in a tissue after 4 days of growth, with an isotropic stress of 1kPa for the right one [39].

4.1 Unconstrained growth of a spheroid

We start with simple considerations on a spherical spheroid.

4.1.1 Population dynamics

We consider a population of cells, the number of which n varies by division and apoptosis, of respective rates k_d and k_a . We can write a master equation describing the time evolution of the probability that the population has n cells

$$\frac{\partial p_n}{\partial t} = k_d[(n-1)p_{n-1} - np_n] + k_a[(n-1)p_{n+1} - np_n] \quad (4.1)$$

Multiplying by n and summing on all n , we get

$$\sum_n n \frac{\partial p_n}{\partial t} = k_d \sum_n \{n(n-1)p_{n-1} - n^2 p_n\} + k_a \sum_n \{n(n+1)p_{n+1} - n^2 p_n\}$$

One should be more cautious about the special cases $n = 0$ and $n = 1$, but we leave this reflection to the reader. We obtain thus a dynamic equation for the mean value $\langle n \rangle$

$$\begin{aligned} \frac{\partial \langle n \rangle}{\partial t} &= k_d [\langle n(n+1) \rangle - \langle n^2 \rangle] + k_a [\langle n(n-1) \rangle - \langle n^2 \rangle] \\ &= (k_d - k_a) \langle n \rangle \end{aligned} \quad (4.2)$$

If $k_d > k_a$, the mean number of cells grows exponentially as $\langle n \rangle = n_0 e^{(k_d - k_a)t}$

We can calculate also the variance (and more generally here all higher moments with a generating function), by multiplying the equation by n^2 and summing on n again

$$\begin{aligned} \frac{\partial \langle n^2 \rangle}{\partial t} &= k_d [\langle n(n+1)^2 \rangle - \langle n^3 \rangle] + k_a [\langle n(n-1)^2 \rangle - \langle n^3 \rangle] \\ &= 2 \langle n^2 \rangle (k_d - k_a) + (k_d + k_a) \langle n \rangle \end{aligned} \quad (4.3)$$

The fluctuation around the mean value is $\delta n = n - \langle n \rangle$, and the variance is obtained as

$$\begin{aligned} \frac{\partial \langle \delta n^2 \rangle}{\partial t} &= \frac{\partial \langle n^2 \rangle}{\partial t} - 2 \langle n \rangle \frac{\partial \langle n \rangle}{\partial t} \\ &= \langle n \rangle (k_d + k_a) + 2 \langle \delta n^2 \rangle (k_d - k_a) \end{aligned} \quad (4.4)$$

If at a time t we have exactly n cells, then $\langle \delta n^2 \rangle = 0$ and in the following times $\Delta t \ll 1$

$$\langle \delta n^2(t + \Delta t) \rangle = (k_d + k_a)n\Delta t,$$

such that δn has a diffusive behavior, but where the "diffusion" coefficient depends on the value of n at the time t of the measure.

Such behavior can also be described by a (chemical) Langevin equation

$$\frac{dn}{dt} = (k_d - k_a)n + \sqrt{(k_d + k_a)n} \xi(t), \quad (4.5)$$

where $\xi(t)$ is a white noise with zero mean $\langle \xi(t) \rangle = 0$ and delta-correlated in time $\langle \xi(t)\xi(t') \rangle = \delta(t - t')$. This supposes that we work at long times compared to the typical division/apoptosis time, such that the noise is not correlated in time, nor the different divisions or apoptosis events.

If one considers a small volume V around the position \mathbf{r} , we can similarly write an equation for the density $\rho(\mathbf{r}, t) \equiv \frac{n}{V}$, including the flux of cells \mathbf{r}

$$\frac{\partial \rho}{\partial t} + \nabla(\rho \mathbf{v}) = (k_d - k_a)\rho + \sqrt{\rho(k_d + k_a)} \xi(\mathbf{r}, t) \quad (4.6)$$

with

$$\langle \xi(\mathbf{r}, t)\xi(\mathbf{r}', t') \rangle = \delta(t - t')\delta(\mathbf{r} - \mathbf{r}').$$

4.1.2 Application: growth of an incompressible spheroid

We consider a spheroid made of cells considered as a single component of density $\rho = \text{cte}$ and we neglect noise. The (4.6) reduces then simply to $\nabla \cdot \mathbf{v} = k_d - k_a \equiv k$, and even though the tissue is incompressible, the divergence of the velocity is not zero (unless $k_d = k_a$ exactly). There is therefore a constant flux of material in the spheroid.

We consider that the division properties of the spheroid depend on the radius r only, and that cells divide in an external layer of thickness λ , and undergo apoptosis in the center, where the nutrient concentration is small, as depicted schematically on Fig. 4.2a.

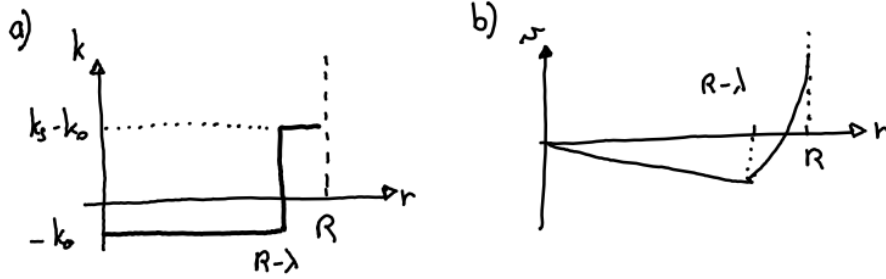


Figure 4.2: Growth of an incompressible spheroid. (a) Profile of the proliferation rate in the spheroid. (b) Radial velocity profile in the spheroid.

The equation can be written in spherical coordinates, which reads

$$\frac{1}{r^2} \frac{\partial}{\partial r} (r^2 v) = k(r).$$

If k is constant, a solution is $v = \frac{kr}{3} + \frac{A}{r^2}$. In the central region of the spheroid, we have $v(r) = -k_0 \frac{r}{3}$ and $A = 0$ to avoid divergence in the center $r = 0$ and in the external region $v = (k_s - k_0) \frac{r}{3} - \frac{k_s (R_\lambda)^3}{3r^2}$ by continuity of the velocity. The profile of the velocity is sketched on Fig. 4.2b.

Over growth, $v(R) > 0$ is positive and decreases in time to eventually vanish in stationary state. At the surface, we have

$$v(R) = \frac{dR}{dt} = (k_s - k_0) \frac{R}{3} - k_s \frac{(R - \lambda)^3}{3R^2} \quad (4.7)$$

The number of cells is $\rho \frac{4}{3}\pi R^3 = N$. Multiplying the equation above by $4\pi R^2 \rho$, we get

$$\frac{dN}{dt} = -k_0 N + k_s N_s, \quad \text{with } N_s = \rho(V - V_\lambda) \quad (4.8)$$

where $V_\lambda = \frac{4}{3}\pi R^3 - \frac{4}{3}\pi(R - \lambda)^3$ is the volume of the external layer of thickness λ .

- if $R < \lambda$, $\frac{dR}{dt} = (k_s - k_0) \frac{R}{3}$: we get an exponential growth of the tissue (contributed only by the external layer).
- if $R \gg \lambda$, $\frac{dR}{dt} = k_s \lambda - \frac{k_0 R}{3}$, giving $R = R_0 [1 - e^{-k_0 t/3}]$, such that growth is linear at the beginning ($t \ll k_0^{-1}$) and saturates at $R_0 = \frac{3\lambda k_s}{k_0}$.

Experimentally, the results above have been observed in growing spheroids made of mouse colon carcinoma cell lines (CT26) [39, 40], as shown on Figs. 4.3 and 4.4.

4.2 Coupling between stress and proliferation

4.2.1 Homeostatic pressure

In general, one may expect a coupling between the rate of tissue growth and the local density: at higher density, the tissue may reduce its proliferation rate. In our continuous settings, this can be expressed by a

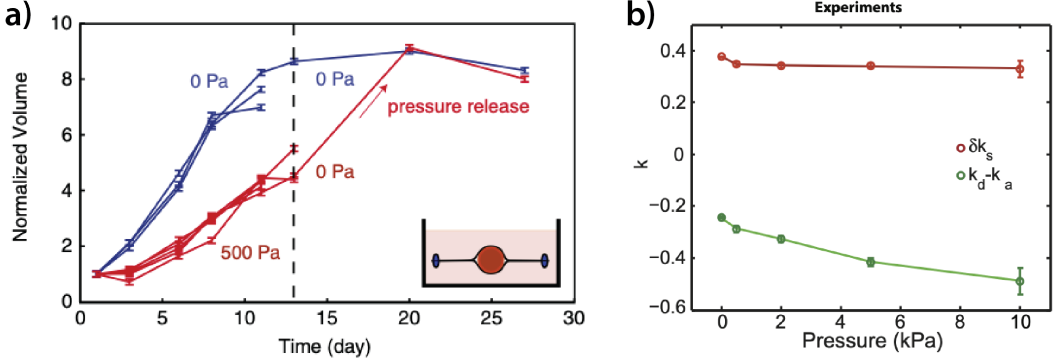


Figure 4.3: Growth of a cellular spheroid under stress [39]. (A) Time evolution of the volume of a spheroid with no stress and under stress. (B) Dependence of the rate of proliferation at the surface and in the bulk of a spheroid as function of the isotropic stress applied.

simple linear relationship

$$k_d - k_a = -\kappa \frac{\rho - \rho_H}{\rho_H} \quad (4.9)$$

where κ is an inverse timescale which quantifies the sensitivity of the tissue proliferation to local density and ρ_H is the density for which the division and apoptosis rates exactly balance each other, see Fig. 4.4a. The equation above can be seen as the first term in a Taylor expansion of the rate of cell division and apoptosis in the cell density.

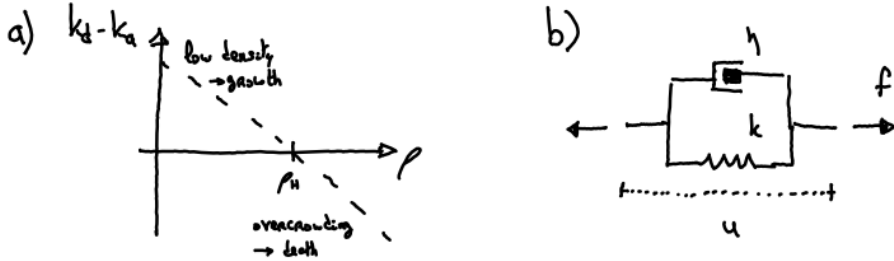


Figure 4.4: (a) Proliferation rate $k_d - k_a$ in the tissue as function of the local density ρ . (b) Rheological diagram of a Maxwell viscoelastic material of viscosity η and elasticity k .

In parallel, one may also expect the isotropic part of the stress to be sensitive to cell density. This can be captured by an equation of state for the pressure P in the tissue:

$$P = P_H + \chi \frac{\rho - \rho_H}{\rho_H} \quad (4.10)$$

where χ is a bulk elastic modulus. This equation simply states that cells have a preferred cell volume (or area in 2D), and deviations from this volume generates a pressure. The pressure P_H is called homeostatic pressure, and is the pressure obtained at the homeostatic point $\rho = \rho_H$, where cell death and cell division exactly balance each other.

While the (4.10) corresponds to an elastic behavior, the effect of cell divisions and cell death on long timescales is to fluidify the tissue, as nicely predicted in [41].

Combining the two equations (4.9) and (4.10) with the cell density balance (4.6) (neglecting the noise term):

$$\frac{DP}{Dt} + \kappa \frac{\rho}{\rho_H} (P - P_H) = -\chi \frac{\rho}{\rho_H} \partial_k v_k \quad (4.11)$$

where $\frac{DP}{Dt} = \partial_t P + v_k \partial_k P$ is the convected (or Lagrangian) time derivative of the pressure. In fact this equation is analog, for $\rho \sim \rho_H$ to the one describing a Maxwell viscoelastic material $(1 + \tau \frac{d}{dt}) = \eta \frac{du}{dt}$, of

viscoelastic timescale $\tau = \eta/k$, as depicted on Fig. 4.4b. Here the equivalent of the viscoelastic timescale, above which the tissue transitions from a solid to a fluid behavior, is $1/\kappa$ and its effective viscosity χ/κ .

4.2.2 Application: expansion of a proliferating confined tissue

As an application, we study here the expansion of a 2-dimensional proliferating tissue along the x -direction, confined in the y -direction between two plates, as depicted on the Fig. 4.5. It is supposed to have an infinite extension in the direction $x \rightarrow +\infty$, has a velocity v_x along x and a moving boundary of constant velocity v_0 .

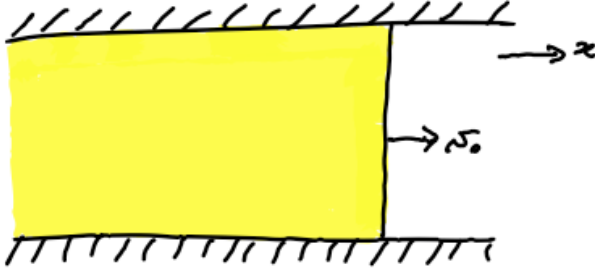


Figure 4.5: Two-dimensional proliferating tissue, confined between two plates.

The cell density conservation equation reads

$$\partial_t \rho + \partial_x(\rho v_x) = (k_d - k_a)\rho \quad (4.12)$$

As discussed above, we assume that proliferation depends locally on the density of the tissue

$$k_d - k_a = -\frac{1}{\tau} \frac{\rho - \rho_H}{\rho_H} \quad (4.13)$$

with τ a typical timescale for cell division.

The constitutive equation for the stress in the tissue reads

$$\sigma_{xx} = -P_H - \chi \frac{\rho - \rho_H}{\rho_H} \quad (4.14)$$

where P_H is the homeostatic pressure in the tissue and χ a bulk elastic modulus. The proliferative pressure P_H is assumed to be uniform across the tissue.

Here we furthermore assume that the tissue feels a friction force when it flows on its substrate, and we characterize it with a friction coefficient ξ , leading to the following force balance equation

$$\partial_x \sigma_{xx} = \xi v_x \quad (4.15)$$

From now on, we restrict ourselves to small deviations from the homeostatic density ρ_H , such that $\rho = \rho_H + \delta\rho$, with $\delta\rho \ll \rho_H$. Linearizing the cell density conservation equation, we obtain

$$\partial_t \delta\rho + \rho_H \partial_x v_x = -\frac{1}{\tau} \delta\rho \quad (4.16)$$

We now rewrite this last equation in the referential of the moving boundary of constant velocity v_0 by introducing the variable $z = x - v_0 t$. This leads to the following equivalence $\partial_t \rightarrow -v_0 \partial_z$ and $\partial_x \rightarrow \partial_z$, and the following equation in z

$$-v_0 \partial_z \delta\rho + \rho_H (\partial_z v_z) = -\frac{1}{\tau} \delta\rho$$

The velocity field $v_z = v_x$ can be calculated from the force balance equation

$$-\frac{\chi}{\rho_H} \partial_x \delta\rho = \xi v_x \quad (4.17)$$

which yields the following new equation for the cell density

$$-v_0 \partial_z \delta\rho - \frac{\chi}{\xi} (\partial_z^2 \delta\rho) = -\frac{1}{\tau} \delta\rho$$

For a small boundary velocity v_0 , this equation simplifies into

$$-\frac{\chi}{\xi} \partial_z^2 \delta\rho + \frac{1}{\tau} \delta\rho = 0 \quad (4.18)$$

We can identify a characteristic length

$$\lambda = \sqrt{\chi\tau/\xi}$$

, and using the fact that the stress at the boundary $z = 0$ should vanish and the cell density shall not diverge for $z \rightarrow -\infty$, the only possible solution has the following form

$$\delta\rho = C e^{\frac{z}{\lambda}} \quad (4.19)$$

with C a constant to determine. The stress follows as

$$\sigma_{xx} = -P_H - \chi \frac{C}{\rho_H} e^{z/\lambda},$$

and using $\sigma_{xx}(z = 0) = 0$, we get $C = -P_H \frac{\rho_H}{\chi}$. The velocity is therefore deduced as

$$v_x = \frac{\partial_z \sigma_{xx}}{\xi} = -\frac{\chi \partial_z \delta\rho}{\xi \rho_H} = \frac{P_H}{\xi} \lambda e^{z/\lambda} \quad (4.20)$$

$$= P_H \frac{1}{\sqrt{\xi\chi\tau}} e^{z/\lambda} \quad (4.21)$$

Finally, this allows us to calculate the expansion velocity v_0

$$v_0 = v_x(z = 0) = P_H \frac{1}{\sqrt{\xi\chi\tau}} \quad (4.22)$$

This equation shows that the speed of expansion of the tissue is slowed down by the friction on the substrate, as expected, and by the tissue bulk modulus, as cell density increases. In this model, all the tissue growth happens in a boundary layer near the interface of length $\lambda = \sqrt{\chi\tau/\xi}$. Further away from this interface, the pressure relaxes to the homeostatic pressure and there is no net cell division, and therefore no growth.

Bibliography

- [1] Pierre-Gilles De Gennes, Françoise Brochard-Wyart, David Quéré, et al. *Capillarity and wetting phenomena: drops, bubbles, pearls, waves*, volume 336. Springer, 2004.
- [2] Malcolm S Steinberg. Reconstruction of tissues by dissociated cells. *Science*, 141(3579):401–408, 1963.
- [3] Philip L Townes and Johannes Holtfreter. Directed movements and selective adhesion of embryonic amphibian cells. *Journal of experimental zoology*, 128(1):53–120, 1955.
- [4] Ramsey A Foty, Cathie M Pfleger, Gabor Forgacs, and Malcolm S Steinberg. Surface tensions of embryonic tissues predict their mutual envelopment behavior. *Development*, 122(5):1611–1620, 1996.
- [5] Ramsey A Foty and Malcolm S Steinberg. The differential adhesion hypothesis: a direct evaluation. *Developmental biology*, 278(1):255–263, 2005.
- [6] Ramsey A Foty, Gabor Forgacs, Cathie M Pfleger, and Malcolm S Steinberg. Liquid properties of embryonic tissues: measurement of interfacial tensions. *Physical review letters*, 72(14):2298, 1994.
- [7] C Norotte, F Marga, A Neagu, I Kosztin, and G Forgacs. Experimental evaluation of apparent tissue surface tension based on the exact solution of the Laplace equation. *European Physical Letters*, 81(4):46003, January 2008.
- [8] JMt Mitchison and MM Swann. The mechanical properties of the cell surface. *J. exp. Biol.*, 31(3):443–460, 1954.
- [9] Karine Guevorkian, Marie-Josée Colbert, Mélanie Durth, Sylvie Dufour, and Françoise Brochard-Wyart. Aspiration of biological viscoelastic drops. *Physical review letters*, 104(21):218101, 2010.
- [10] Francois Mazuel, Myriam Reffay, Vicard Du, Jean-Claude Bacri, Jean-Paul Rieu, and Claire Wilhelm. Magnetic flattening of stem-cell spheroids indicates a size-dependent elastocapillary transition. *Physical review letters*, 114(9):098105, 2015.
- [11] Jose E Perez, Irène Nagle, and Claire Wilhelm. Magnetic molding of tumor spheroids: emerging model for cancer screening. *Biofabrication*, 13(1):015018, 2020.
- [12] Albert K Harris. Is cell sorting caused by differences in the work of intercellular adhesion? a critique of the steinberg hypothesis. *Journal of theoretical biology*, 61(2):267–285, 1976.
- [13] François Graner and James A Glazier. Simulation of biological cell sorting using a two-dimensional extended potts model. *Physical review letters*, 69(13):2013, 1992.
- [14] G Wayne Brodland. The differential interfacial tension hypothesis (dith): a comprehensive theory for the self-rearrangement of embryonic cells and tissues. *J. Biomech. Eng.*, 124(2):188–197, 2002.
- [15] K Vijay Kumar. The actomyosin cortex of cells: A thin film of active matter. *Journal of the Indian Institute of Science*, 101(1):97–112, 2021.
- [16] Jean-Léon Maître and Carl-Philipp Heisenberg. Three functions of cadherins in cell adhesion. *Current Biology*, 23(14):R626–R633, 2013.

- [17] Jean-Léon Maître, Hélène Berthoumieux, Simon Frederik Gabriel Krens, Guillaume Salbreux, Frank Jülicher, Ewa Paluch, and Carl-Philipp Heisenberg. Adhesion functions in cell sorting by mechanically coupling the cortices of adhering cells. *science*, 338(6104):253–256, 2012.
- [18] M Lisa Manning, Ramsey A Foty, Malcolm S Steinberg, and Eva-Maria Schoetz. Coaction of intercellular adhesion and cortical tension specifies tissue surface tension. *Proceedings of the National Academy of Sciences*, 107(28):12517–12522, 2010.
- [19] Andrew R Harris, Loic Peter, Julien Bellis, Buzz Baum, Alexandre J Kabla, and Guillaume T Charras. Characterizing the mechanics of cultured cell monolayers. *Proceedings of the National Academy of Sciences*, 109(41):16449–16454, 2012.
- [20] Matthias Merkel, Raphaël Etournay, Marko Popović, Guillaume Salbreux, Suzanne Eaton, and Frank Jülicher. Triangles bridge the scales: Quantifying cellular contributions to tissue deformation. *Physical Review E*, 95(3):032401, 2017.
- [21] S Ishihara, K Sugimura, SJ Cox, Isabelle Bonnet, Y Bellaïche, and F Graner. Comparative study of non-invasive force and stress inference methods in tissue. *The European Physical Journal E*, 36(4):1–13, 2013.
- [22] Reza Farhadifar, Jens-Christian Röper, Benoit Aigouy, Suzanne Eaton, and Frank Jülicher. The influence of cell mechanics, cell-cell interactions, and proliferation on epithelial packing. *Current Biology*, 17(24):2095–2104, 2007.
- [23] Douglas B Staple, Reza Farhadifar, J-C Röper, Benoit Aigouy, Suzanne Eaton, and Frank Jülicher. Mechanics and remodelling of cell packings in epithelia. *The European Physical Journal E*, 33(2):117–127, 2010.
- [24] Edouard Hannezo, Jacques Prost, and Jean-Francois Joanny. Theory of epithelial sheet morphology in three dimensions. *Proceedings of the National Academy of Sciences*, 111(1):27–32, 2014.
- [25] Hisao Honda, Masaharu Tanemura, and Tatsuzo Nagai. A three-dimensional vertex dynamics cell model of space-filling polyhedra simulating cell behavior in a cell aggregate. *Journal of theoretical biology*, 226(4):439–453, 2004.
- [26] Satoru Okuda, Takashi Miura, Yasuhiro Inoue, Taiji Adachi, and Mototsugu Eiraku. Combining turing and 3d vertex models reproduces autonomous multicellular morphogenesis with undulation, tubulation, and branching. *Scientific reports*, 8(1):1–15, 2018.
- [27] Jean-Léon Maître, Hervé Turlier, Rukshala Illukkumbura, Björn Eismann, Ritsuya Niwayama, François Nédélec, and Takashi Hiiragi. Asymmetric division of contractile domains couples cell positioning and fate specification. *Nature*, 536(7616):344–348, 2016.
- [28] Jorge Nocedal and Stephen J Wright. Conjugate gradient methods. *Numerical optimization*, pages 101–134, 2006.
- [29] Sybren Ruurds De Groot and Peter Mazur. *Non-equilibrium thermodynamics*. Courier Corporation, 2013.
- [30] Karsten Kruse, Jean-Francois Joanny, Frank Jülicher, Jacques Prost, and Ken Sekimoto. Generic theory of active polar gels: a paradigm for cytoskeletal dynamics. *The European Physical Journal E*, 16(1):5–16, 2005.
- [31] Paul M Chaikin, Tom C Lubensky, and Thomas A Witten. *Principles of condensed matter physics*, volume 10. Cambridge university press Cambridge, 1995.
- [32] Vikram Deshpande, Antonio DeSimone, Robert McMeeking, and Pierre Recho. Chemo-mechanical model of a cell as a stochastic active gel. *Journal of the Mechanics and Physics of Solids*, 151:104381, 2021.

- [33] P Yo Chou. On velocity correlations and the solutions of the equations of turbulent fluctuation. *Quarterly of applied mathematics*, 3(1):38–54, 1945.
- [34] Pierre-Gilles De Gennes and Jacques Prost. *The physics of liquid crystals*. Number 83. Oxford university press, 1993.
- [35] S Fürthauer, M Strempel, Stephan W Grill, and Frank Jülicher. Active chiral fluids. *The European physical journal E*, 35(9):1–13, 2012.
- [36] G Duclos, C Blanch-Mercader, V Yashunsky, G Salbreux, J-F Joanny, J Prost, and Pascal Silberzan. Spontaneous shear flow in confined cellular nematics. *Nature physics*, 14(7):728–732, 2018.
- [37] Guillaume Duclos, Christoph Erlenkämper, Jean-François Joanny, and Pascal Silberzan. Topological defects in confined populations of spindle-shaped cells. *Nature Physics*, 13(1):58–62, 2017.
- [38] Morgan Delarue, Fabien Montel, Danijela Vignjevic, Jacques Prost, Jean-François Joanny, and Giovanni Cappello. Compressive stress inhibits proliferation in tumor spheroids through a volume limitation. *Biophysical journal*, 107(8):1821–1828, 2014.
- [39] Fabien Montel, Morgan Delarue, Jens Elgeti, Laurent Malaquin, Markus Basan, Thomas Risler, Bernard Cabane, Danijela Vignjevic, Jacques Prost, Giovanni Cappello, et al. Stress clamp experiments on multicellular tumor spheroids. *Physical review letters*, 107(18):188102, 2011.
- [40] Morgan Delarue, Fabien Montel, Ouriel Caen, Jens Elgeti, Jean-Michel Siaugue, Danijela Vignjevic, Jacques Prost, Jean-François Joanny, and Giovanni Cappello. Mechanical control of cell flow in multi-cellular spheroids. *Physical review letters*, 110(13):138103, 2013.
- [41] Jonas Ranft, Markus Basan, Jens Elgeti, Jean-François Joanny, Jacques Prost, and Frank Jülicher. Fluidization of tissues by cell division and apoptosis. *Proceedings of the National Academy of Sciences*, 107(49):20863–20868, 2010.